AD NUMBER

AD063407

LIMITATION CHANGES

TO:

Approved for public release; distribution is unlimited.

FROM:

**Distribution authorized to U.S. Gov't. agencies and their contractors;
Administrative/Operational Use; 30 SEP 1954.
Other requests shall be referred to Office of Naval Research, 875 North Randolph Street, Arlington VA 22203-1995.**

AUTHORITY

ONR ltr, 26 Oct 1977

Carnegie Institute of Technology

Department of Physics

INVESTIGATIONS OF THERMAL AND ELECTRICAL PROPERTIES OF SOLIDS AT VERY LOW TEMPERATURE

FINAL REPORT

CONTRACT N6ORI-47 - T.O.3

Department of Physics

Carnegie Institute of Technology

Contract Nóori-47 Task Order 3

Project number NR 016-403

Office of Naval Research

INVESTIGATIONS OF THERMAL AND ELECTRICAL PROPERTIES OF SOLIDS AT VERY LOW TEMPERATURE

FINAL REPORT

Submitted by

S. A. Friedberg

Principal Investigator

Period of Contract

April 15, 1946 to September 30, 1954

TABLE OF CONTENTS

The work described in this report was initiated by Dr. I. Estermann, principal investigator for this Contract from 1946 until 1952. Supervision of the work was carried on by Dr. J. E. Zimmerman, principal investigator from 1952 to 1953, and by Dr. S. A. Friedberg, principal investigator from 1953 to 1954.

The following individuals were associated with research activities of this Contract for the periods indicated:

Mr. D. L. Burk (1951 - 1954)

Dr. Anna Foner Cohen (1946 - 1950)

Mr. F. J. Darnell (1951 - 1954)

Miss Doane Douthett (1954)

Dr. I. Estermann (1946 - 1952)

Dr. S. A. Friedberg (1948 - 1951 and 1952 - 1954)

Dr. J. E. Goldman (1951 - 1954)

Mr. C. T. Linder (1948 - 1950)

Dr. P. M. Marcus (1952 - 1954)

Dr. E. Mendoza (1952 - 1953)

Mr. W. K. Robinson (1953 - 1954)

Dr. Julia Randall Weertman (1946 - 1951)

Dr. J. E. Zimmerman (1949 - 1953)

INVESTIGATIONS OF THERMAL AND ELECTRICAL PROPERTIES OF SOLIDS AT VERY LOW TEMPERATURES

I. INTRODUCTION

The research program carried out under Contract N6ori-47, T. O. 3 during the period April 15, 1946 to September 30, 1954 has included work on a rather wide range of topics in solid state and low temperature physics. Many of the results of these investigations have already been presented in the form of technical reports and published articles. This report will, therefore, include merely the briefest statements of these results together with appropriate references. Emphasis will be placed rather on the presentation of results hitherto unpublished, most of which have been obtained during the last two years. In several instances these results serve to indicate the status of work which is being continued beyond the date of termination of this contract.

II. CALORIMETRY

The heat capacities of several metals and non metals have been determined as functions temperature in the liquid helium range as well as between liquid hydrogen temperatures and about 200°K. Vacuum calorimeters described in Technical Reports 7[27] and 8[28] were used for many of these measurements. Recently a larger calorimeter designed along conventional lines has been constructed and employed in work between $\sim 1.5^{\circ}$ and 22°K. Temperature measurement from $\sim 10^{\circ}$K upwards has been by means of a L and N platinum resistance thermometer. In much of the helium temperature work germanium resistance thermometers, developed in this laboratory[1,2], were used. Recently carbon composition resistances of the Allen-Bradley type have been used extensively over the range 1.5° to 22°K.

The way in which solids take up thermal energy, as revealed by specific heat observations, is indicative of many fundamental aspects of their

structure. Such features as the density of electronic energy states at the Fermi surface or the presence of significant interaction among magnetic ions are typical of the types of information gained in the investigations to be described. It is convenient to group the results according to the kind of material studied and the temperatures at which the measurements were made.

A. Metals Below 4.2°K.[3,4,5,11,28,29]

C_p has been determined as a function of temperature between ~ 1.8° and 4.2°K for specimens of Cr, Ti, Zr, Mg, Cu (pure and impure), and the alloy Ni_3Mn in both the ordered (ferromagnetic) and disordered (paramagnetic) forms. In each case it has been possible to represent $C_p(\simeq C_v)$ as $\gamma T + \beta T^3$, i.e. the sum of an electronic and a lattice contribution. The coefficient γ yields directly the density of electronic energy states at the Fermi level for a given metal while β provides a value of the Debye characteristic temperature, θ, of the lattice.

The results for Cr, Ti, Zr, Mg and impure Cu have already been reported.[5,28] The γ values for Ti and Zn were found to be intermediate between those associated with non-transition metals such as Al and Mg and the large values typical of other transition elements. This is in accord with current ideas of the shape of the d-band in transition metals. More striking, however, is the fact that for Cr a γ value of only 3.8×10^{-4} cal/deg^2 mol was observed. In other words the Fermi level for Cr lies at a point where the density of states of the d-band is quite low. Existing calculations of d-band shapes by Slater and others for later members of the first transition sequence, e.g. copper, do in fact predict a minimum in the density of states curve at the position near the middle corresponding to the Fermi level of Cr. The γ value for Cr may, therefore, be

interpreted in a simple way if the shape of the d band in copper may be presumed to have the same general features as that of the earlier members of the first transition group.

The results of measurement on Ni_3Mn specimens in the ordered and disordered states are plotted in Fig. 1 as C_p/T vs T^2. The γ value for the disordered alloy (paramagnetic) is 22.4×10^{-4} cal/mol deg^2. This is twice as large as the γ for the ordered (ferromagnetic) material namely 11.7×10^{-4} cal/mol deg^2. The implications of this result have been discussed by Goldman[11]. It is in harmony with the idea that in the ferromagnetic material the half-band of d-electrons with one spin is full or nearly full so that only d-electrons in the partly filled half-band of opposite spin may contribute to the specific heat.

Earlier measurements of C_p for copper performed in this laboratory[28] were done on a specimen containing 0.5 o/o lead impurity. The electronic heat was little affected by this addition, the observed γ, 1.8×10^{-4} cal/deg^2 mol, being in good agreement with that reported by Keesom and Kok[31] for pure material. The Θ value observed was, however, somewhat lower than the value 335° given by Keesom and Kok, as might be expected from the known small value of Θ for the lead impurity.

New measurements have been made on a copper specimen of rather high purity (99.99 o/o) which had been annealed at 400°C for 48 hours. A germanium thermometer was used. The results are plotted as C_p/T vs T^2 in Fig. 2 and as C_p vs T in Fig. 3. The constants associated with the smooth curves drawn through the experimental points are $\gamma = 1.8 \times 10^{-4}$ cal/deg^{2}mol and $\Theta = 343°$. The general agreement with the results of Keesom and Kok is rather good. The small discrepancy in the values of Θ appears to be outside the limits of experimental error. A Θ of 343 has also been reported

for pure copper recently by Corak et al[32].

B. Metals Above 15°K.[27,9,10]

C_p has been measured for chromium, titanium, zirconium, and hafnium between ~ 15°K and 200°K. The individual specimens are described in Table I.

The results for titanium are shown in Fig. 4. In Table II values of C_p taken from the smooth curve drawn through the experimental points are given. Corresponding C_v values have also been tabulated. These were calculated by means of the formula: $C_v = C_p \left(1 - \frac{9\alpha^2 V}{K C_p^2} C_p T \right) = C_p \left(1 - 5.7 \times 10^{-6} C_p T \right)$. C_v values corrected for the electronic contribution are also shown as well as the effective Debye temperatures deduced therefrom. These results are in excellent agreement with those of Johnston and Kothen[33] in the region in which they overlap.

The data for zirconium are presented in Fig. 5 and Table III. Values of C_v, of C_v minus the electronic part, and effective Debye θ's are also tabulated. Agreement between these results and those of Johnston and Skinner[34] for zirconium is quite good. This specimen and the titanium specimen described above are the same ones on which measurements had been previously made below 4.2°K.[5,28]

The hafnium results are given in Fig. 6 and Table IV, the latter containing also C_v, corrected C_v, and effective θ values. The electronic contribution used to correct C_v values to those representing the lattice heat alone has been taken from preliminary measurements of the electronic heat determined below 4.2°K in this laboratory. The value of $\gamma (6 \times 10^{-4} \frac{\text{cal}}{\text{mol deg}^2}$ quoted here is provisional. The final results of these measurements at liquid helium temperature will be reported at a later date.

In Fig. 7 the effective Debye temperatures θ for Ti, Zr, and Hf

TABLE I

Heat Capacity Specimens

METAL	AT.WT.	SPECIMEN WT.	PURITY	PRINC. IMPURITIES
Ti	47.90	27.416 gm.	>99 o/o	
Zr	91.22	19.429	99.5 o/o	Na
Hf	178.6	46.420	98 o/o	Zr(~2 o/o)
Cr	52.01	16.111	99.9 o/o	Al,Cu,Si

TABLE II

HEAT CAPACITY OF TITANIUM

$T(^{\circ}K)$	$C_p \left(\frac{cal}{^{\circ}mol}\right)$	$C_v \left(\frac{cal}{^{\circ}mol}\right)^{*}$	$C_{v_{latt}} \left(\frac{cal}{^{\circ}mol}\right)^{**}$	$\theta_D(^{\circ}K)$
22.5	.119	.119	.100	372
25	.176	.176	.155	360
30	.304	.304	.279	354
35	.458	.458	.429	356
40	.650	.650	.617	357
45	.879	.879	.842	357
50	1.142	1.142	1.101	355
55	1.413			
60	1.674	1.673	1.623	355
65	1.932			
70	2.187	2.185	2.127	357
75	2.428			
80	2.659	2.656	2.590	358
85	2.872			
90	3.085	3.080	3.005	359
95	3.288			
100	3.476	3.469	3.386	358
105	3.648			
110	3.810	3.801	3.710	356
115	3.959			
120	4.098	4.086	3.987	355
125	4.229			
130	4.346			
135	4.456			
140	4.560	4.544	4.428	352
145	4.650			
150	4.736			
155	4.813			
160	4.886	4.864	4.731	353
165	4.951			
170	5.031			
175	5.068			
180	5.119	5.097	4.948	354
185	5.166			
190	5.220	5.191	5.037	355
195	5.273			
200	5.320	5.288	5.122	353

$^{*}C_v = C_p (1 - 5.7 \times 10^{-6} C_p T)$

$^{**}C_{v_{latt}} = C_v - 8.29 \times 10^{-4} T$

TABLE III

HEAT CAPACITY OF ZIRCONIUM

T(°K)	$C_p\left(\frac{cal}{mol}\right)$	$C_v\left(\frac{cal}{mol}\right)^{*}$	$C_{v_{latt}}\left(\frac{cal}{mol}\right)^{**}$	θ_D(°K)
20	0.2441	0.2441	0.2303	252
25	0.4836	0.4836	0.4663	247
30	0.7888	0.7888	0.7680	247
35	1.136	1.136	1.112	247
40	1.502	1.502	1.474	248
45	1.850	1.850	1.819	251
50	2.183	2.182	2.147	254
55	2.512	2.511	2.473	255
60	2.822	2.821	2.779	255
65	3.103	3.102	3.057	256
70	3.371	3.370	3.322	255
75	3.610			
80	3.831	3.829	3.773	254
85	4.028			
90	4.202	4.199	4.137	253
95	4.352			
100	4.498	4.494	4.425	252
105	4.610			
110	4.709	4.704	4.628	254
115	4.808			
120	4.892	4.887	4.804	255
125	4.972			
130	5.038			
135	5.103			
140	5.174	5.167	5.070	256
145	5.240			
150	5.305			
155	5.376			
160	5.446	5.437	5.326	242
165	5.517			
170	5.573			
175	5.625			
180	5.667	5.656	5.532	220
185	5.695			
190	5.714			
195	5.737			
200	5.751	5.738	5.600	223

$^{*}C_v = C_p\,(1 - 1.88 \times 10^{-6} C_p T)$

$^{**}C_{v_{latt}} = C_v - 6.92 \times 10^{-4} T$

TABLE IV

HEAT CAPACITY OF HAFNIUM

T(°K)	$C_p\left(\frac{cal}{°mol}\right)$	$C_v\left(\frac{cal}{°mol}\right)^{*}$	$C_v\Big\|_{latt}\left(\frac{cal}{°mol}\right)^{**}$	θ_D(°K)
10	0.0423	0.0423	0.0363	234
15	0.1654	0.1654	0.1564	215
20	0.4040	0.4040	0.3920	210
25	0.7733	0.7733	0.7583	206
30	1.235	1.235	1.217	204
35	1.708			
40	2.185	2.183	2.159	202
45	2.620			
50	3.012	3.007	2.977	201
55	3.374			
60	3.682	3.673	3.637	197
65	3.940			
70	4.174	4.161	4.119	198
75	4.382			
80	4.582	4.564	4.516	194
85	4.767			
90	4.932	4.908	4.854	186
95	5.075			
100	5.186	5.157	5.097	180
105	5.267			
110	5.344	5.310		
115	5.413			
120	5.467	5.428	5.356	177
125	5.510			
130	5.548			
135	5.583			
140	5.617	5.569	5.485	181
145	5.637			
150	5.667			
155	5.694			
160	5.717	5.660	5.564	188
165	5.740			
170	5.767			
175	5.787			
180	5.817	5.751	5.643	188
185	5.844			
190	5.860			
195	5.883			
200	5.906	5.830	5.710	184

$^{*}C_v = C_p(1 - 1.08 \times 10^{-5} C_p T)$

$^{**}C_v\Big|_{latt} = C_v - 6.0 \times 10^{-4} T$

have been plotted as functions of temperature. The decrease of Θ_D with increasing atomic weight in this sequence of Group IVa metals is as expected on the basis of specific heat theory. Note that Θ_D is defined such that $k\,\Theta_D = h\,\nu_{max}$ where ν_{max} is the maximum allowed frequency of atomic vibration in the solid. We may write the equation of motion of an atom vibrating about its equilibrium lattice site as $M\ddot{X} + K X = 0$ where X is the displacement, K the force constant, and M the atomic mass. The frequency of atomic oscillation is simply $\nu = \frac{1}{2\pi}\sqrt{\frac{K}{M}}$. We may reasonably expect, therefore, that Θ_D will also be proportional to $\frac{1}{M^{1/2}}$. For members of a group of elements having such similar properties (including elastic constants) as do those of Group IVa the product $\Theta_D M^{1/2}$ or $\Theta_D A^{1/2}$, where A is the atomic weight, may be expected to have nearly the same value. That this is so is seen in Table V.

	Θ_D	A	$\Theta_D A^{1/2}$
Ti	355	47.9	2460
Zr	250	91.2	2390
Hf	190	178.6	2530

The Θ_D values used here are those observed in the range where this parameter is relatively temperature-independent.

As has been briefly noted in an earlier report[9], the present measurements on hafnium fail to confirm the existence of an anomalous peak in C_p at 60°K described by Cristescu and Simon[35]. This result may well reflect significant differences in purity between the specimen used in this work and that used in the earlier measurements. Hafnium of even 98 o/o purity has only been recently made available. Not only is the specific heat of reasonably pure hafnium found to be regular but, as we have seen, it is

quite consistent with those of titanium and zirconium. This is very encouraging from the point of view of the theory of lattice specific heats in terms of which anomalous behavior is completely inexplicable.

The experimental findings for chromium are given in Fig. 8 and Table VI. These results overlap those of Anderson[36] obtained in the range 56° to 300°K. The agreement between the two sets of measurements is quite satisfactory. Particular emphasis has been placed in the present work on the temperature range in the vicinity of 120°K. It is in this region that Fine et al[26] have observed an anomaly in Young's Modulus for chromium. As was mentioned in an earlier report,[10] no specific heat anomaly has been detected in the region of interest at least to the limit of resolution of the measurements. An anomalous peak in C_p having a width of no more than about 5° could probably be observed.

Effective values of Θ_D for chromium are plotted against temperature in the upper part of Fig. 7. A maximum value, $\Theta_D = 515$, is reached at about 30°K. Below this temperature, Θ_D decreases continuously with temperature reaching a value of 487 at 20°K. In the region below 4°K earlier measurements gave a Θ_D of 418. This appears to be quite consistent with the trend observed above 20°.

C. Non-Metals.

(1) Germanium[7,27,6,38]

The specific heat of the semiconductor germanium was measured for several specimens of very different purity. Measurements between 20° and 200°K, described in detail in Technical Report No. 7,[27] indicate only a very slight dependence of C_p on impurity content. They do not reveal any anomalous features such as the peak between 40° and 140°K reported in 1934 by Cristescu and Simon[35]. Measurements to below 4°K, described in

TABLE VI

HEAT CAPACITY OF CHROMIUM

T(°K)	C_p $\left(\frac{cal}{g\ mol}\right)$	C_v $\left(\frac{cal}{g\ mol}\right)^*$	$C_v)_{latt}$ $\left(\frac{cal}{g\ mol}\right)^{**}$	θ_D(°K)
20	0.0387	0.0387	0.0312	487
25	0.0646	0.0646	0.0552	509
30	0.1033	0.1033	0.0921	515
35	0.1582	0.1582	0.1451	515
40	0.2453	0.2453	0.2303	505
45	0.3519	0.3519	0.3351	500
50	0.4875	0.4875	0.4683	493
55	0.6618	0.6618	0.6412	484
60	0.8555	0.8555	0.8331	478
65	1.049	1.049	1.025	476
70	1.256	1.256	1.230	473
75	1.462	1.461	1.433	472
80	1.679	1.678	1.648	470
85	1.901	1.900		
90	2.108	2.107	2.073	466
95	2.311	2.309		
100	2.515	2.513	2.476	462
105	2.700			
110	2.867	2.864	2.823	462
115	3.031			
120	3.186	3.182	3.137	461
125	3.335			
130	3.474	3.469		
135	3.612			
140	3.738	3.732	3.680	458
145	3.848			
150	3.961			
155	4.068			
160	4.168	4.159	4.099	456
165	4.261			
170	4.355			
175	4.442			
180	4.516	4.504	4.437	451
185	4.587			
190	4.649			
195	4.694			
200	4.723	4.708	4.633	461

$^*C_v = C_p(1 - 3.23 \times 10^{-6} C_p T)$

$^{**}C_v)_{latt} = C_v - 3.74 \times 10^{-4} T$

Technical Report #28, suggest that in very impure degenerate germanium specimens an electronic contribution to the specific heat may be observable.

(3) Normal Spinels

Ferrites have the general molecular formula $(M^{++})(Fe^{+++})_2O_4$, where M^{++} may be Mn^{++}, Fe^{++}, Zn^{++}, etc. They crystallize in the spinel structure in which the metallic ions may occupy lattice sites of two non-equivalent types, the tetrahedral (A) and octahedral (B) sites surrounded by four and six oxygen atoms respectively. Néel has successfully described the magnetic properties of many ferrites by assuming the exchange interaction of ions on A-sites with ions on B-sites (A-B interactions) to be antiferromagnetic and much stronger than A-A or B-B interactions. The latter are also assumed generally to be antiferromagnetic although little direct evidence has been available until recently to indicate their actual nature.

Zinc and cadmium ferrites are the only ones possessing the so-called "normal" spinel structure in which all B-sites are occupied by Fe^{+++} ions and all A sites by divalent ions. Since Zn^{++} and Cd^{++} are diamagnetic the only magnetic interaction present in either $ZnFe_2O_4$ or $CdFe_2O_4$ should be of the weak B-B type. Consequently long-range ordering of Fe^{+++} spins is to be expected only at low temperatures.

Corliss and Hastings[37] have carried out neutron diffraction studies of $ZnFe_2O_4$ over a wide temperature range. They find evidence of short-range spin ordering at hydrogen temperature and the actual appearance of a complicated long-range order among Fe^{+++} spin at helium temperatures. In order to study the thermal character of this transition and actually to fix the transition temperature more closely we have measured the specific heat of $ZnFe_2O_4$ over the range 1.3 to 200°K.

The specimen, kindly provided by Dr. V. C. Wilson of the General Electric Company, had been prepared by sintering the mixed oxides (with slight excess of ZnO) at 1200°for four hours. Twenty four grams of the crushed material were used. Copper capsules held the specimen during the measurements, one equipped with a platinum resistance thermometer to cover the range 10 to 200°K; another with a carbon resistance thermometer for use between 1.3 and 20°K. Heat capacities of the filled capsules (including He exchange gas) were determined by the vacuum calorimeter method in these ranges. In a separate series of measurements, the capsule corrections were determined in the same intervals. The capsule technique was used at helium temperatures in spite of its difficulties only after preliminary experiments with a one-piece specimen showed the thermal relaxation time of the sintered material to be too long for calorimetric purposes.

Calibration of the carbon thermometer, particularly between 4.2 and 10°K, presents a special problem. The method used follows that of Clement[38]. Numerous calibration points were obtained at helium and hydrogen temperatures. An equation of the form $\sqrt{\frac{\log R}{T}} = a + b \log R$ (where R is resistance, T is temperature, a and b are constants) was fitted approximately to these points by fixing b at some appropriate value. Systematic deviation from this relation was found when a was plotted vs log R. Interpolation in the 4.2° to ~10°K interval was done on this plot by drawing the best curve consistent with the deviation. In practice, temperatures were obtained from observed resistance by summing terms calculated from the formula and corrections read from the deviation plot.

The general nature of the results is indicated in Fig. 9 where representative C_p values are plotted against T between 1.2 and 200°K. An anomalous peak having its maximum at about 9°K is evident. The peak is

shown in detail in Fig. 10. A transition temperature, T_N, of 9°K agrees well with the neutron diffraction results as does the existence of the prominent "tail" above T_N indicating significant short range spin order up to 25°K and probably beyond.

There is little doubt that the observed anomaly is actually associated with a magnetic transition of a cooperative type. It is, however, unusual in several respects. Repeated measurements in the transition region with increased resolution (smaller ΔT's) failed to show C_p assuming the exceptionally large values found in a typical λ-shaped anomaly. No conclusive evidence was found for a discontinuity in $\frac{dC_p}{dT}$ much less for any sort of discontinuity in C_p itself. Such discontinuities would characterize ideal transitions of the third and second order respectively. It seems unlikely that systematic experimental errors, in particular any inadequacy of the interpolated thermometer calibration used in this region, could mask any of these features if they were actually present. Immediate assignment of this anomaly to a simple category does not, therefore, appear feasible.

A specific heat maximum without a discontinuity in $\frac{dC_p}{dT}$ is to be expected for an anomaly of the Schottky type. Such an anomaly is not associated with a cooperative transition but is rather characteristic of a system possessing two or more energy states whose spacing is of the order kT and is independent of their relative occupation. That the anomaly in $ZnFe_2O_4$ is not of the Schottky type in spite of its superficial resemblance to such a peak follows, of course, from the existence of long range spin order below 9°K. It is also interesting to note that the temperature dependence of C_p below the maximum is quite incompatible with that expected of a Schottky anomaly.

In the region from 4.2°K down to 1.2°K, where the thermometer calibration is most reliable, C_p is found to vary quite closely as $T^{3/2}$. An exponential decrease would probably be evident at these temperatures were the anomaly of the Schottky type.

It is quite possible that the observed specific heat anomaly is rounded and broadened as compared with those found in typical cooperative transitions because the specimen was not of uniform composition. Slightly different transition temperatures in different parts of the specimen might account for this behavior and could result from local variations in the number and position of neighboring magnetic ions. Partial inversion and deviations from ideal stoichiometry would contribute to such a picture. It is likely that the detailed shape of the anomaly in $ZnFe_2O_4$ depends to some extent on the exact composition and mode of preparation of a given specimen. For this reason it is hoped that it will be possible in the near future to carry out measurements of specific heat for other samples of $ZnFe_2O_4$ prepared in different ways. On the other hand, it seems quite unlikely that such materials could have transition temperatures much different from that obtained by noting the position of the maximum in the anomaly reported here, i.e. $T_N \simeq 9°K$. The quantity $k\,T_N$ determined from these results is thought, therefore, to provide a direct measure of the strength of the B-B interaction in $ZnFe_2O_4$.

A satisfactory separation of lattice and magnetic contributions to the observed specific heat has not proved possible in this case. If the short range order tail of the anomaly is assumed to be negligible at temperatures above about 50°K then one might attempt to extrapolate the lattice contribution back from the C_p curve measured above this temperature. At best this is a crude process . However, if it is carried out and a mag-

netic contribution obtained by subtraction, we may estimate the magnetic entropy gained in going from the ordered antiferromagnetic state at 0°K to the completely disordered paramagnetic state at very high temperatures. This estimate turns out to be considerably lower than the theoretical value $2R \ln (2S + 1) = 2R \ln 6$ expected for 2 Fe^{+++} ions (in $^6S_{5/2}$ states) per mole of $ZnFe_2O_4$. If, as the neutron diffraction results indicate, short range order is significant even at 180°K the magnetic anomaly has a much larger tail than would be inferred from inspection of the C_p curve. This would probably account for much of the entropy missing in the simple estimate.

As was mentioned above, C_p is found to approach zero approximately as $T^{3/2}$ below 4.2°K. Such a temperature dependence is expected on the basis of spin wave theory for the specific heats of ferro- or ferrimagnets cooled well below their Curie points. For ideal antiferromagnets, on the other hand, the spin wave specific heat should vary as T^3 at temperatures well below the Néel point. Ordinarily the spin wave approximation is considered valid only at temperatures below about one-tenth that of the cooperative transitions. Recent work by Eisele and Keffer[39] suggests, however, that in antiferromagnets, at least, the thermal properties typical of spin waves may persist to higher temperatures. The possibility exists, therefore, that in $ZnFe_2O_4$ below 4.2°K a spin wave contribution to the specific heat is actually being observed. If this is so then the fact that the specific heat varies nearly as $T^{3/2}$ rather than as T^3 must be explained since the material is presumed to be antiferromagnetic. It is conceivable that partial inversion of the spinel structure sufficient to broaden the transition as suggested above could also account for this ferrimagnetic manifestation.

Guided by the results obtained for $ZnFe_2O_4$ it was decided to measure the specific heat of the analogous normal spinel, $ZnCr_2O_4$, over the same temperature range. In this material all B sites are presumably occupied by Cr^{+++} ions each with a spin of 3/2. Again weak B-B interaction is the only one present and is expected to affect long range spin ordering at some low temperature.

The specimen, obtained from the Naval Ordnance Laboratory through the kindness of Doctors J. S. Smart and F. McGuire, was in the form of a fine powder. Measurements were carried out on fourteen grams of the material in the same manner described earlier. The experimental values of C_p are plotted against temperature in Fig. 11. A sharp peak having its maximum at $11.8^\circ K$ is strikingly evident. A detailed plot of this region is given in Fig. 12. We may identify $11.8^\circ K$ as the Néel point, T_N, of $ZnCr_2O_4$ since subsequent neutron diffraction studies actually show that the long range spin order existing below this temperature is antiferromagnetic in nature.

The anomaly in this case has the appearance commonly associated with a cooperative transition. The largest measured value of C_p is nearly 14 cal/mole°. Above $11.8^\circ K$, C_p falls rapidly but continuously. A large short-range order tail makes the magnetic contribution a major portion of the total specific heat up to temperatures as high as $35^\circ K$ and possibly above. Below $11.8^\circ K$, C_p falls rapidly with decreasing temperature as shown. Preliminary measurements down to $2.0^\circ K$ (not indicated in Fig. 12) suggest that, in fact, C_p is proportional to T^3 below about $9^\circ K$. If this result is borne out by more extensive measurements in this region now in progress an interpretation in terms of spin waves appears quite possible. As mentioned above, the spin wave contribution to the specific heat of an antiferromagnet should vary as T^3.

An attempt has been made to separate lattice and magnetic contributions to the specific heat of Zn Cr_2O_4 in order that the magnetic entropy increase might be estimated for the transition. We may begin by assuming that for temperatures above 11.8°K Zn Cr_2O_4 is paramagnetic with exchange coupling between Cr^{+++} ions. Van Vleck[40] has shown that for $kT >> \mu H_i$, where H_i is the molecular field by which the coupling may be represented, the specific heat may be written $\frac{\text{const } H_i^2}{T^2}$. If in this region the lattice specific heat varies as T^3 then we may write for the observed total $C = \frac{b}{T^2} + AT^3$. A plot of CT^2 vs T^5 should give a straight line of slope A and intercept b. Such a plot for Zn Cr_2O_4 is shown in Fig. 13. From it we see that between 12.6° and 25°K the total specific heat is well represented by $C_p\left(\frac{\text{cal}}{°\text{mol}}\right) = \frac{310}{T^2} + 7.3 \times 10^{-5}T^3$. Above 25°K the observed values fall below such a curve. This is reasonable since here the lattice contribution is rising more slowly than as T^3. If one assumes that the second term in the above expression is valid down to 0°K then, by subtraction, values for the magnetic contribution may be obtained over the whole range from 0° to 25°K. Above 25°K $C_p(\text{mag})$ will be just $\frac{310}{T^2}$. The integral $\Delta S = \int_0^\infty \frac{C_p(\text{mag})}{T}\, dT$ may be evaluated by combined graphical and analytical methods. The result is $\Delta S \simeq 2.5 \frac{\text{cal}}{°\text{mol}}$. This presumably is the entropy gained in going from the completely ordered antiferromagnetic state to the completely disordered paramagnetic state. We should expect: $\Delta S = 2R \ln(2S + 1) = 2R \ln 4$ or $5.6 \frac{\text{cal}}{°\text{mol}}$, where the factor 2 results from two Cr^{+++} ions being contained in one mole of Zn Cr_2O_4.

The reason for the discrepancy in entropy values deduced from the observations and predicted theoretically is not obvious. The assumptions underlying the analysis of the data outlined above appear reasonable

enough so that at least some of the discrepancy may be considered real. Several conceivable situations could account for it. For example, the spin arrangement assumed just below 11.8°K may not be unique, a second transition at some still lower temperature being needed to produce complete order. Detailed analysis of the neutron diffraction results should enable one to confirm or reject such a picture.

It is interesting to note that the large tail on the observed specific heat anomaly makes it assymetric in the sense that the entropy gained above T_N is actually somewhat larger than that gained below T_N as the temperature is raised from 0°K. Recently, Domb[41] has shown that similar behavior is to be expected for Ising models in which a given ionic moment interacts strongly with only a small number of neighbors. This is reasonable, of course, since for very large values of this number all order must be long range in nature. On the other hand, a very small number of interactions would give rise primarily to short range order and so to a large tail on the anomalous peak. While considerations such as these can provide little quantitative information about the number of interacting neighbors in Cr_2O_4, the qualitative notion that this number is small appears reasonable. Detailed analysis of the neutron diffraction results should clarify this point.

III. Semiconductors

A. Earlier work (1946 to 1951)[12,13,14,15,24]

The original objective of the program of semiconductor research in this laboratory was extension to very low temperatures of measurements of electrical resistance and galvanomagnetic effects in germanium and silicon. This work was undertaken as part of a cooperative effort to understand the properties of these substances at a time when few experiments had been carried to liquid nitrogen temperatures (77°K) and practically none to temperatures

below 77°K.

All of the early work was of necessity carried out with polycrystalline specimens. The electrical resistances, ρ , and Hall constants, R, of a series of such specimens containing added donor or acceptor impurities in widely varying amounts were determined between 300° and 4°K. A third derived quantity, the Hall mobility, $\mu_H = \frac{R}{\rho}$, was calculated from these results for most of the specimens.

These materials exhibited properties placing them in several rather distinct groups. The most impure specimens (1 to 17 At. o/o impurity) behaved essentially as poor metals. The purest materials ($\sim$1 part in 10^7 impurity) showed properties fitting qualitatively the theoretical picture of an impurity semiconductor in which the carrier concentration is always low enough to permit the use of Maxwell-Boltzmann statistics. Specimens of intermediate purity also behaved as impurity semiconductors but in many instances the transition to degenerate carrier characteristics became apparent within the temperature interval covered. The temperature variation of mobility for the purer materials could generally be interpreted in terms of the combined effects of lattice and ionized impurity scattering, the former predominating at high temperatures, the latter becoming important at low temperatures.

Full descriptions of this work have been given in Technical Reports Nos. 1, 2, 3, and 4 (see Refs.23 and24 for detailed titles). Generally speaking the observations were qualitatively described by a simple model in which carriers were supplied by either donor or acceptor impurities and in which the transition from Maxwell-Boltzman to Fermi-Dirac statistics was only crudely treated. Several of the results, anomalous on this picture, are probably attributable to the presence in these early

specimens of appreciable concentrations of minority impurities. This fact introduces an indeterminacy which makes analysis of these experiments, beyond that contained in the cited reports, unprofitable.

Following the work just outlined an extensive investigation of the magnetoresistance effects in polycrystalline germanium was made between 12° and 300°K[15]. The details are given in Technical Report No. 5[25]. The electrical resistance was measured as a function of applied magnetic field strength and the relative orientation of electric and magnetic fields. The results were compared with the phenomenological theory of Seitz[42] and several serious discrepancies noted. It is now recognized that these stem from the fact that the energy band structure of germanium is much more complicated than that assumed in the theory.

The large changes of electrical resistance with temperature found at low temperatures for rather pure germanium were exploited for thermometric purposes in work which has been described in Technical Report No. 8[28]. Resistance thermometers of high sensitivity in the liquid helium region were obtained from indium-doped germanium ingots by a systematic sampling technique. They were used extensively in calorimetry below 4.2°K.

The work described thus far was carried out in the period from 1946 to 1951. In 1953 it was decided to resume these investigations for several reasons: (1) Single crystal germanium of well-defined impurity content had become available; (2) The theoretical picture of the band structure of germanium was in the process of clarification; (3) The temperature range available for experimental purposes had been extended to well below 1°K.

The work which will now be discussed was in progress at the close of the period covered by this report (September 1954). Those phases of it

which were completed at that time will be outlined. The program has been continued under the auspices of both the Office of Naval Research and the National Science Foundation. A separate report will be issued soon containing detailed discussions of the experimental methods as well as the results and their interpretation.

B. Work since 1953

The present program consists essentially of a survey of the temperature dependence of the resistivity of germanium from $0.2^{\circ}K$ to room temperature and of the Hall constant from $1.3^{\circ}K$ to room temperature. Particular attention has been given the dependence of these properties on magnetic and electric fields. Both single crystal and polycrystalline germanium specimens covering a wide range of impurity concentrations are being used. Measurement of these electrical properties provides material for a critical examination of several features of the conventional model of an impurity semiconductor.

1. Experimental Equipment and Methods

For temperatures above $1.3^{\circ}K$ the samples were placed directly in baths of liquid helium, hydrogen, nitrogen, or methane, using dewar arrangements of the type shown in previous reports. Accurate temperature determination is then possible by measurement of the bath vapor pressure. Temperatures below $1.3^{\circ}K$ were obtained by adiabatic demagnetization of paramagnetic salts, temperatures being measured by a carbon resistance thermometer. After testing Allen-Bradley radio resistors and films fabricated from colloidal graphite suspensions, it was found that 1000 Ω IRC radio resistors have satisfactory resistance characteristics in the region 0.1° to $4.2^{\circ}K$. Calibration of such a thermometer was carried out by comparison with magnetic susceptibility measurements on the paramagnetic salt, as well as by a thermo-

dynamic method[23]. Some of the details of the demagnetization apparatus are shown in Figs. 14 and 15.

The circuit for electrical measurements on the samples (Fig. 16) is similar to that described previously. The extremely high resistance of the purer samples necessitated a few changes, including the use of standare resistances in values up to 10 megohms.

Magnetic fields up to 5500 gauss were furnished by an iron core electromagnet arranged to rotate about a vertical axis for magnetoresistance measurements. Fields for the magnetic cooling procedure were provided by the same magnet, which was mounted on rails for quick removal after demagnetizations.

In Table VII, the characteristics of the specimens employed in this work are summarized.

The polycrystalline specimens were 34FA, 12S, and 35P, originally from Purdue University; 83E, origin unknown; S2, obtained from Dr. Shockley of the Bell Telephone Laboratories; and A2 from a melt prepared at this laboratory. The single crystals were obtained from Dr. B. Sawyer of the Bell Telephone Laboratories.

TABLE VII

DATA FOR GERMANIUM SAMPLES

SAMPLE	STRUCTURE	TYPE	IMPURITY	RESISTIVITY AT 300°K (ohm-cm)	IMPURITY CONCENTRATION* (/cm^3)
12S	Poly-	n	P (?)	.023	1.2×10^{17}
83E	Crystalline	P	(Unknown)	.053	8.1×10^{16}
35P	"	P	.006 at .o/o Al	.038	3.7×10^{16}
34PA	"	n	.04 at .o/o Sb	.012	1.1×10^{17}
A2	"	P	.001 at .o/o In	.078	2.5×10^{16}
S2	"	n	(Unknown)	0.33	4.7×10^{15}
B12	Single	P	Ga	1.18	1.6×10^{15}
B22	Crystal	n	Sb	1.58	2.2×10^{15}
B32	"	n	As	.0046	1.7×10^{19}
B42	"	n	-	28	6.2×10^{13}

*Difference between majority and minority carrier concentrations, as calculated from room temperature Hall Constant.

2. Resistivity

Although measurements on several of the polycrystalline samples have been reported previously,[23,24] only new data will be considered in this discussion. Extension of resistance measurements to low temperatures necessitates an investigation of the current density as a function of applied electric field, since it has been shown[14] that the resistance of germanium in the helium range is a function of the electric field. This dependence is being studied in detail at the present time. It is found that above a critical electric field a sample undergoes "breakdown", in which the current density increases several orders of magnitude for small increases in electric field. This has been interpreted[43,44] as an avalanche effect due to impact ionization of impurity atoms by current carriers. The carrier multiplication process has been followed directly by means of Hall effect determinations which will not be described here. Current density as a function of electric field is shown for two samples in Figs. 17 and 18 to illustrate the effects of temperature and transverse magnetic fields on the critical electric field. Simple considerations based on the ballistics of charged particles in crossed electric and magnetic fields permit the estimation of carrier mean free paths and times from such data.

Magnetoresistance measurements have been carried out only for single crystal specimens for which the effects are quite large. At 4°K, for example, the resistance of a pure specimen may increase by several hundred percent in a field of 5000 gauss. These observations have been made for various orientations of current and magnetic field with respect to the crystalline axes and one another. The results together with their interpretation in the light of theory which takes into account the complex energy band structure of germanium will be presented in the aforementioned report as will the results

of the breakdown studies.

Figures 19, 20, and 21 show the resistivities of the specimens described in Table I as functions of temperature. In all cases, the applied electric fields have been well below the critical breakdown values.

3. Hall Constant

As in previously reported measurements[23,24] the Hall constant depends on the magnetic field strength, generally decreasing as the field increases. In the present investigation data were taken as functions of field, so that by extrapolation a value of Hall constant could be obtained for zero field. Such zero field values are given in Figures 22 and 23. Data for the magnetic field dependence will be reserved for presentation with magnetoresistance results. The extremely high resistance of the purer samples at helium temperatures, together with the necessity for keeping the electric fields small, results in very small currents, $\sim 10^{-8}$ amps, and correspondingly small Hall voltages. Difficulties associated with the measurement of such small voltages accounts for the scarcity of data below 10°K.

4. Hall Mobility

The Hall mobility is defined by

$$\mu_H \equiv \frac{R}{\rho} = \frac{r}{nec}\, ne\mu = \frac{r}{c}\mu$$

where r is a constant characteristic of the resistive scattering processes and the degree of degeneracy of the particular sample and μ is the actual or drift mobility. A plot of μ_H as a function of temperature is shown in Fig. 24.

5. Discussion

All of the samples discussed here exhibit impurity conduction primarily, with the exception of B42, which shows intrinsic conduction above 280°K. We therefore wish to interpret the results in terms of charge carriers orig-

inating from impurity atoms and their associated energy levels. We shall formulate the discussion in terms of donor impurities, which provide excess electrons; similar arguments hold for acceptor impurities, the sources of deficit electrons, or holes.

A donor impurity atom with five electrons in unfilled shells will replace a germanium atom substitutionally and satisfy the covalent bond structure with four of its electrons. The fifth electron is bound to the impurity ion in a hydrogen-like state with energy $\sim$ .01eV below the bottom of the conduction band. Electrons in those levels are easily excited thermally into the conduction band and account for the conductivity at room temperature and below. As the temperature is decreased, these electrons will drop back into the bound states and the resistivity increases sharply. At the lowest temperatures, however, this model gives a resistance which increases without limit, since at 0°K electrons will exist only in the full valence band of the germanium matrix and in bound impurity states. This prediction is in conflict with the experimental results of this research, which generally show a levelling off of the resistivity as the temperature is lowered through the helium region. These data may be easily explained on the basis of conduction in a band of impurity levels[45] arising from the interactions of the bound states of the impurity atoms. If the impurity concentration is great enough to allow appreciable overlap of the bound state wave functions, the interaction will cause the bound energy levels to expand into a band. This band will contain a number of states equal to twice the number of impurity atoms, and will furnish a mechanism for conduction at 0°K, since no activation energy is required. The experimental results and this interpretation are in agreement with those of Ing and Gliessman[45]. There arises

the question whether interactions are sufficiently large at low impurity concentrations to account for the observed results. Calculations of the energy levels for random impurities in a regular lattice by James and Ginzbarg[46] and Aigrain and Jancovici[47] show that the banding effect may be considerable for impurity concentrations down to $\sim 10^{16}$ /cc. Concentration of impurities as determined from the Hall constant is actually the difference between donor and acceptor concentrations. Observations of impurity band effects for samples with quoted impurity concentrations of $\sim 10^{15}$ /cc or less should then be considered as arising at least in part from compensated impurities not shown in the Hall constant. This is particularly true for the polycrystalline samples reported here and those of Hung and Gliessman, all of which were prepared before 1950, and may explain why impurity band effects have not been observed in the purer samples investigated elsewhere[48].

The impurity band model also serves to explain the decrease in activation energy with increasing impurity concentration[49]. The disappearance of the activation energy at a concentration of $\sim 1.5 \times 10^{17}$ /cc is in agreement with calculations of impurity density necessary for overlap of impurity and conduction bands.

Most of the samples show a straight line in the helium region on plots of log resistivity vs 1/T, corresponding to a temperature dependence of the form $\rho = A\, e^{\frac{\Delta\epsilon}{2kT}}$ with $\Delta\epsilon \sim 10^{-4}$ eV. This is in a temperature range below that at which the impurity electrons are excited into the conduction band. This exponential expression may be only an approximation, and reflect a temperature dependence of mobility, rather than a change in carrier concentration.

The Hall constants show little change from 300°K to 150°K, where those

for the more impure samples begin to rise, the rise starting at a lower temperature the purer the sample. Curves for the less pure samples pass through maxima, decreasing to constant values at the lowest temperatures. Curves for the more pure samples, rising rapidly below $10^{\circ}K$, show evidence of leveling off, but no evidence for a subsequent decrease, which, if present, will occur below $1^{\circ}K$.

This behavior is explained easily on the basis of an impurity band model. At high temperatures the Hall constant characterizes the electrons in the conduction band, at the lowest temperatures the electrons in the donor impurity band. At intermediate temperatures the Hall constant R involves the mobilities μ_c and μ_d, as well as the carrier concentrations, n_c and n_d, in the conduction and donor bands, respectively;

$$R = \frac{r}{e} \frac{n_c \mu_c^2 + n_d \mu_d^2}{(n_c \mu_c + n_d \mu_d)^2}$$

This expression shows a maximum in the transition region in accord with the experimental results.

The mobility curves for the purer samples show the $T^{-3/2}$ dependence expected for lattice scattering, and this extends to quite low temperatures. The less pure samples show evidence of an appreciable ionized impurity scattering, with a $T^{3/2}$ dependence, even at room temperature. The decreasing values at low temperatures may be interpreted as an increasing dependence on impurity scattering, but if the impurity band model is valid a mobility $\mu_H = \frac{R}{\rho}$ does not have a simple meaning in the region where the Hall expression involves more than one conduction process.

IV. Temperature Waves at Low Temperatures[13,19,30]

The diffusivity (ratio of thermal conductivity to specific heat per unit volume) of a metal can be determined by measuring the velocity of

propagation of a sinusoidally varying temperature wave along a rod made from the metal. This technique has been described briefly by Dr. E. Mendoza[18], who also initiated the present program for its perfection during his visit in this department (1952-1953). The temperature variation is generated by a heater at the end of the rod, and the temperature wave is detected by two quickly responding resistance thermometers spaced along the rod (see Fig. 25). Frequencies from 50 to 1000 cycles per second are used. The resistance of each thermometer varies sinusoidally, and the phase difference between these two sine waves is measured. Since the diffusivity of metals at low temperatures is practically independent of temperature, it should be possible to measure it with high accuracy by this method. Measurement of the thermal conductivity is done with the same apparatus and therefore the specific heat can be found.

In Technical Report No. 1C[19,30], Dr. P. M. Marcus has studied the problem of temperature wave propagation with the help of a transmission line analogue and determined the effects of a change in cross section and various terminations of the rod. He finds that these would cause reflections of the temperature wave, necessitating large corrections to the phase measurements at the lower frequencies where the wave length is large. It was also shown that the waves are heavily damped, the damping factor being approximately .002 over one wave length. The wave length is of the order of a few millimeters except for metals at low temperatures where it is several times the length of the rod, or of the order of fifty centimeters for a frequency of one hundred cycles per second. Therefore this technique is restricted to low temperatures. It can be adapted to temperatures below $1^{\circ}K$.

The thermometers and heater each consist of a film of colloidal graphite painted on the rod, which has previously been coated with an insulating film of lacquer (Tuffernell B-165). It has been found that the thermal noise generated by these thermometers is not a problem at liquid helium temperatures after they have been subjected to prolonged outgassing. Better signals are also obtained if the colloidal graphite is rubbed so as to pack it more tightly.

The signal obtained from the thermometers is of the order of one millivolt. In one circuit built by Dr. J. E. Zimmerman, each signal was amplified by a factor of approximately one hundred. One output went to a helipot amplitude control and the other to a phase shifting bridge. The two signals were then mixed and further amplified, the final output going to an oscilloscope. The phase and amplitude controls were adjusted for a null reading on the oscilloscope, and the phase difference of the two signals could then be determined from the setting of the phase shifting bridge. In Zimmerman's other circuit the same phase shifting bridge was used to shift the phase of the signal from the oscillator, which was also the heater power source. This signal was then doubled in frequency and fed into one input of a phase discriminator, the other input of which received the signal from one of the thermometers, and the output of which was measured by a vacuum tube voltmeter. The phase discriminator and vacuum tube voltmeter were used as a null indicator as the calibrated phase shifter was adjusted. The difference of the readings obtained from the two thermometers represented the phase shift of the temperature wave at these two locations.

These two circuits gave results that were accurate to approximately ten percent. One source of error was the phase shifting bridge which could be adjusted to the nearest degree only. Since it was necessary to measure

phase differences as small as five degrees, it was sought to develop a more sensitive bridge. However, it was eventually decided that a null reading was not sensitive enough because of the broadness of the null.

The present circuit (see Figs. 26, 27, 28) is entirely different in principle. Instead of measuring the phase, the time interval between the two signals is measured directly. The signals are first amplified to approximately twenty volts, then clipped and amplified several times to obtain square waves, and finally differentiated. This results in a series of positive and negative pulses from each channel, the time delay from the positive pulse from channel A to that from channel B being the quantity measured. Use is made of a calibrated triggered delay circuit called the phantastron. It is triggered by the leading positive pulse and subsequently generates a delayed pulse. The delay pulse is adjusted to coincide with the pulse from channel B. Better than one percent accuracy is expected with this arrangement.

In order to obtain symmetry of the square wave resulting from the clipped signals, the bias on the first clipper is adjusted until the negative pulse is equidistant in time from the two adjacent positive pulses. The phantastron is used in adjusting the time intervals.

Provision is also made for interchanging channels A and B. By averaging the two time delays obtained, any error due to different phase shift in the two channels is canceled.

A brief description of the circuit will now be given with the help of the block diagram.

When making a measurement, switches 1 and 2 are both in positions a or b, switch 4 is in position a, and switch 3 is on normal. The positive pulse from the leading channel therefore triggers the phantastron while the pulse

from the other channel goes to the phase splitter, the output of which can be selected to give the same polarity as the delay pulse from the phantastron.

For calibration, switches 2 and 5 are both in positions a or b, and switch 3 is on calibrate. One channel, therefore, is completely out of the circuit. With switch 4 at position a, the phantastron is triggered by the positive pulse from the channel being calibrated, while the negative pulse triggers the phantastron when position b is used. The calibration procedure consists of adjusting the delay pulse until it coincides with the next pip from the phase splitter, then changing switches 4 and 6 to see if the same delay is obtained from the other half of the square wave. If there is an error, approximately half of it is corrected by changing the bias of the first clipper stage, and then the symmetry of the square wave is checked again. This process quickly gives a square wave that is symmetrical with the limit of accuracy of the phantastron.

V. Thermal Conductivity of Solids[20,21,22,26]

A series of investigations of the thermal conductivity of various solids between 2° and 30°K is described in Technical Report No. 6[26]. Electrical conductivities were determined for these specimens over the same interval to permit the calculation of Wiedemann-Franz ratios. The results may be summarized briefly as follows:

A. Commercial Alloys[20,21,22,26]

Measurements on monel, inconel, and stainless steel gave Wiedemann-Franz ratios much larger than the theoretical value, the deviations being greater for annealed than for cold worked specimens. These results are consistent with the idea that lattice conductivity is relatively high in these alloys. The thermal conductivity values obtained in this work have

been very useful in the design of cryogenic equipment in this laboratory and elsewhere.

B. 90 o/o Cu - 10 o/o Ni Alloy[20,21,22,26]

Specimens of the same composition but differing as to degree of cold work and grain size were studied. Qualitative interpretation of the differing conductivities have been given in terms of plausible arguments about the influence of cold work upon lattice conduction.

C. Germanium[22,26]

Specimens of varying impurity content showing different non-degenerate electrical properties in the temperature interval 2° to 80°K were studied. No appreciable electronic conductivity was observed. At very low temperatures the effect of impurity concentration was found to be consistent with the theory of lattice conduction.

The work outlined above was completed in 1951. In 1954 it was decided to resume thermal conductivity studies with metals of the hexagonal close-packed structure the particular objects of investigation . At the close of the period covered by this report an improved apparatus for helium and hydrogen range measurements using carbon resistance thermometers was under construction. The program is continuing and it is hoped that with the use of single crystals it will be possible to examine the anisotropy of the thermal conductivity in the pure metals as well as the influence of alloying additions upon that anisotropy.

VI. Miscellaneous Topics

A. The Electrical Resistance of α-Brass

Very little information appears to be available on the low temperature resistance of the important copper-zinc alloys. Requests for such data from another group in our department led to a series of determinations of the re-

sistance of α-Brass between 1.6° and $300^{\circ}K$ the results of which will be summarized briefly. The specimens (30 o/o Zn, 70 o/o Cu) were in the form of drawn wires of circular cross-section (0.101 cm dia., $\sim$ 22 cm long)with attached potential and current leads. Measurements were carried out by a potentiometric method in liquid helium, hydrogen, oxygen, and nitrogen baths as well as at room temperature.

The resistivity of the unannealed material was found to be 7.35×10^{-6} Ωcm at $299^{\circ}K$ and 4.54×10^{-6} Ωcm at $4.2^{\circ}K$ and below, a decrease, $\Delta\rho$, of 2.81×10^{-6} Ωcm. The same specimens annealed for 3 hours at 592° exhibited resistivities of 6.28×10^{-6} Ωcm and 3.47×10^{-6} Ωcm. at $299^{\circ}K$ and $4.2^{\circ}K$ respectively, a decrease, $\Delta\rho$, of 2.81×10^{-6} Ωcm as before. Thus Matthiessen's Rule is obeyed. The room temperature resistivity is within the range 6 to 9×10^{-6} Ωcm reported by several early investigators.

The low temperature data on annealed α-Brass are shown in Fig. 29. For purposes of rough interpolation for temperatures above $\sim 40^{\circ}K$ one may use the Grüneisen formula taking as the characteristic temperature the value $\Theta = 215^{\circ}K$.

B. Laboratory Aids

1. Level indicator for liquid He, H_2, and N_2.

An inexpensive portable level indicator for low boiling point liquids has been in use in this laboratory for several years. Its essential details are shown schematically in Fig. 30. A small box holds the indicating milliammeter (0-20 ma), batteries and switches. The sensitive element, a 56 Ω, 1/2 W carbon composition resistor of the Allen-Bradley type, is mounted at the end 32" x 3/16" dia. inconel tube from the other

end of which emerge the leads which may be connected to the rest of the circuit by a small Jones plug.

In operation, the long probe is inserted slowly into the mouth of the vessel containing the liquid, the range switch having been set to the proper value. Power dissipated in the resistor raises its temperature well above that of the gas through which it passes. Contact with the liquid surface produces a marked increase in the resistance of the sensing element and an easily observed drop in current indicated on the meter. The probe is then suitably marked and withdrawn and the liquid depth or volume determined with the aid of a calibration chart.

2. Bellows manostat

Pressures less than atmospheric may be maintained over liquid refrigerant baths (particularly helium and hydrogen) for extended periods by means of a simple manostat shown in Fig. 31. The essential element is a large sylphon bellows of phosphor bronze which is extended when the reference pressure exceeds that of the bath, causing the pumping line to close. Opening the needle valve separating the reference chamber from the pumping line permits the reduction of the reference pressure by arbitrary amounts.

In operation with a liquid helium bath the manostat provides pressure regulation to about 0.1 mm. Hg. over most of the useful range. A bypass around the manostat is usually included in the circuit to permit pressures below about 2 cm Hg to be reached.

REFERENCES

Publications 1 through 30 describe work done under Contract N6ori-47 T. O. 3, Project NR 016-403.

1. I. Estermann, Phys. Rev. 78, 83(A), (1950). See also: Proceedings of the International Conference on the Physics of Very Low Temperatures, M.I.T.(1949)

2. S. A. Friedberg, Phys. Rev. 82, 769(A), (1950)

3. I. Estermann and S. A. Friedberg, Phys. Rev. 85, 715(A), (1950).

4. S. A. Friedberg, I. Estermann, and J. E. Goldman, Phys. Rev. 85, 375-376 (1952).

5. I. Estermann, S. A. Friedberg, and J. E. Goldman, Phys. Rev. 86, 582-588 (1952).

6. I. Estermann and S. A. Friedberg, Changements de Phases, Paris 1952 p. 312.

7. I. Estermann and J. R. Weertman, Phys. Rev. 83, 228(A) (1951).

8. I. Estermann and J. R. Weertman, J. Chem. Phys. 20, 972-976 (1952).

9. D. Burk and F. J. Darnell, Phys. Rev. 86, 628(A) (1952).

10. J. Weertman, D. Burk, and J. E. Goldman, Phys. Rev. 85, 623(A) (1952).

11. J. E. Goldman, Revs. Mod. Phys. 25, 108 (1953).

12. I. Estermann, A. Foner, and J. A. Randall, Phys. Rev. 71, 484(A) (1947).

13. I. Estermann, A. Foner, and J. A. Randall, Phys. Rev. 72, 530(A) (1947).

14. I. Estermann, A. Foner, and J. E. Zimmerman, Phys. Rev. 75, 1631(A) (1949).

15. A. Foner and I. Estermann, Phys. Rev. 77, 759(A) (1950).

16. I. Estermann and A. Foner, Phys. Rev. 79, 365-372 (1950).

17. D. H. Howling, F. J. Darnell, and E. Mendoza, Phys. Rev. 93, 1416 (1954).

18. E. Mendoza, Phys. Rev. 90, 347(A) (1953).

19. P. M. Marcus, Phys. Rev. 94, 771(A) (1954).

20. J. E. Zimmerman, Phys. Rev. 82, 769(A) (1951).

21. J. Estermann and J. E. Zimmerman, J. Appl. Phys. 23, 578-588 (1952)

22. I. Estermann and J. E. Zimmerman, Proc. Conf. on Heat Conduction, Louvain, 1952.

Items 23 through 30 are Technical Reports issued under Contract N6ori-47 T.O.3, Project NR 016-403 by the Carnegie Institute of Technology.

23. Technical Reports No. 1 and No. 2 entitled respectively Quarterly Prog. Re-

43. Sclar, Burstein, Turner, and Davidson, Phys. Rev. 91, 215(A) (1953); 92, 858(A) (1953).

44. F. J. Darnell and S. A. Friedberg, Bull. Am. Phys. Soc. 30, No. 1, 39 (1955).

45. C. S. Hung and J. R. Gliessman, Phys. Rev. 79, 726, 727 (1950); 96, 1226 (1954).

46. H. M. James and A. S. Ginzbarg, J. Phys. Chem. 57, 840 (1953).

47. P. Aigrain and B. Jancovici, Phys. Rev., to be published.

48. F. H. Geballe and F. J. Morin, Phys. Rev. 95, 1085 (1954)

49. P. P. Debye and E. M. Conwell, Phys. Rev. 93, 693 (1954).

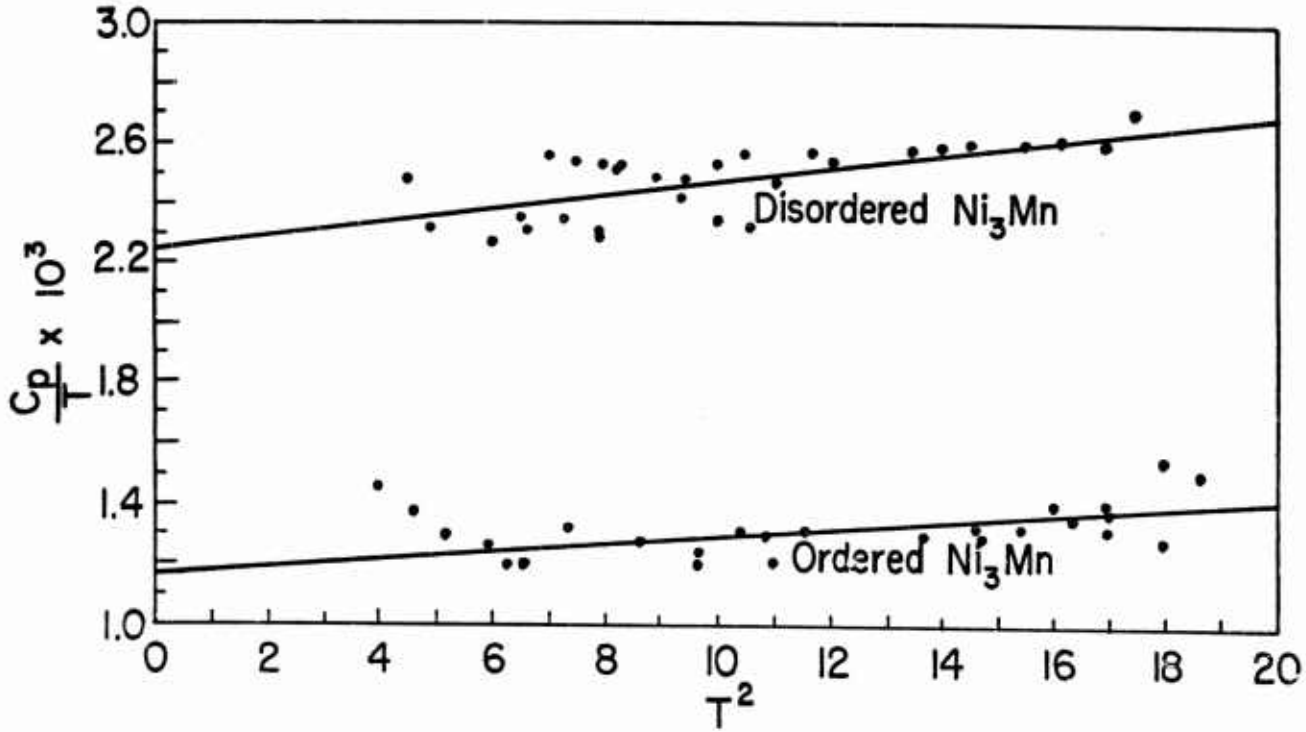
3.0
2.6
2.2
1.8
1.4
1.0
$\frac{C_p}{T} \times 10^3$
Disordered Ni_3Mn
Ordered Ni_3Mn
0
2
4
6
8
10
12
14
16
18
20
T^2

FIGURE 1

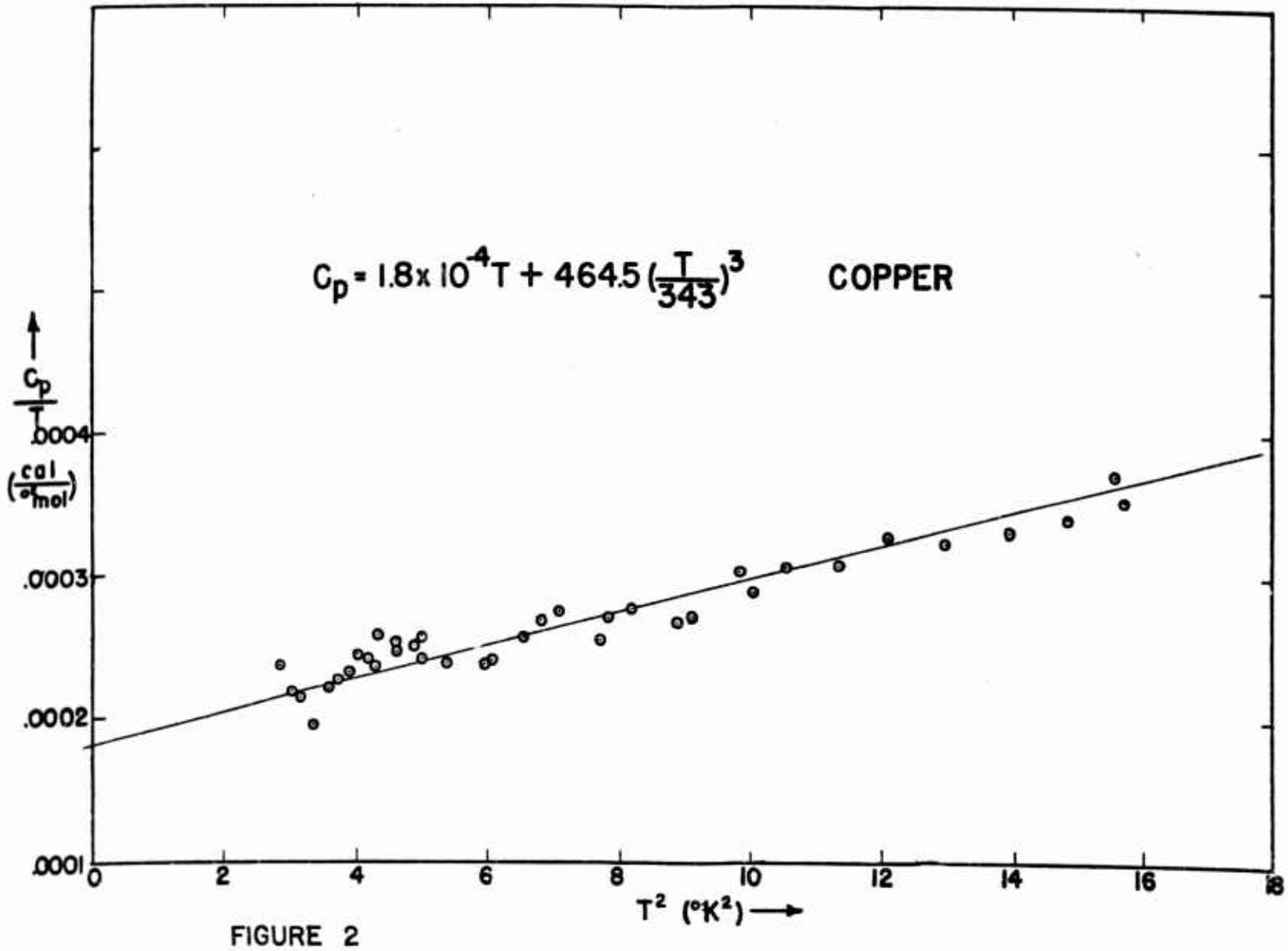
$C_p = 1.8 \times 10^{-4} T + 464.5 \left(\frac{T}{343}\right)^3$ COPPER
$\frac{C_p}{T}$
$\left(\frac{cal}{°K\ mol}\right)$
.0004
.0003
.0002
.0001
0
2
4
6
8
10
12
14
16
18
T^2 (°K²) ⟶

FIGURE 2

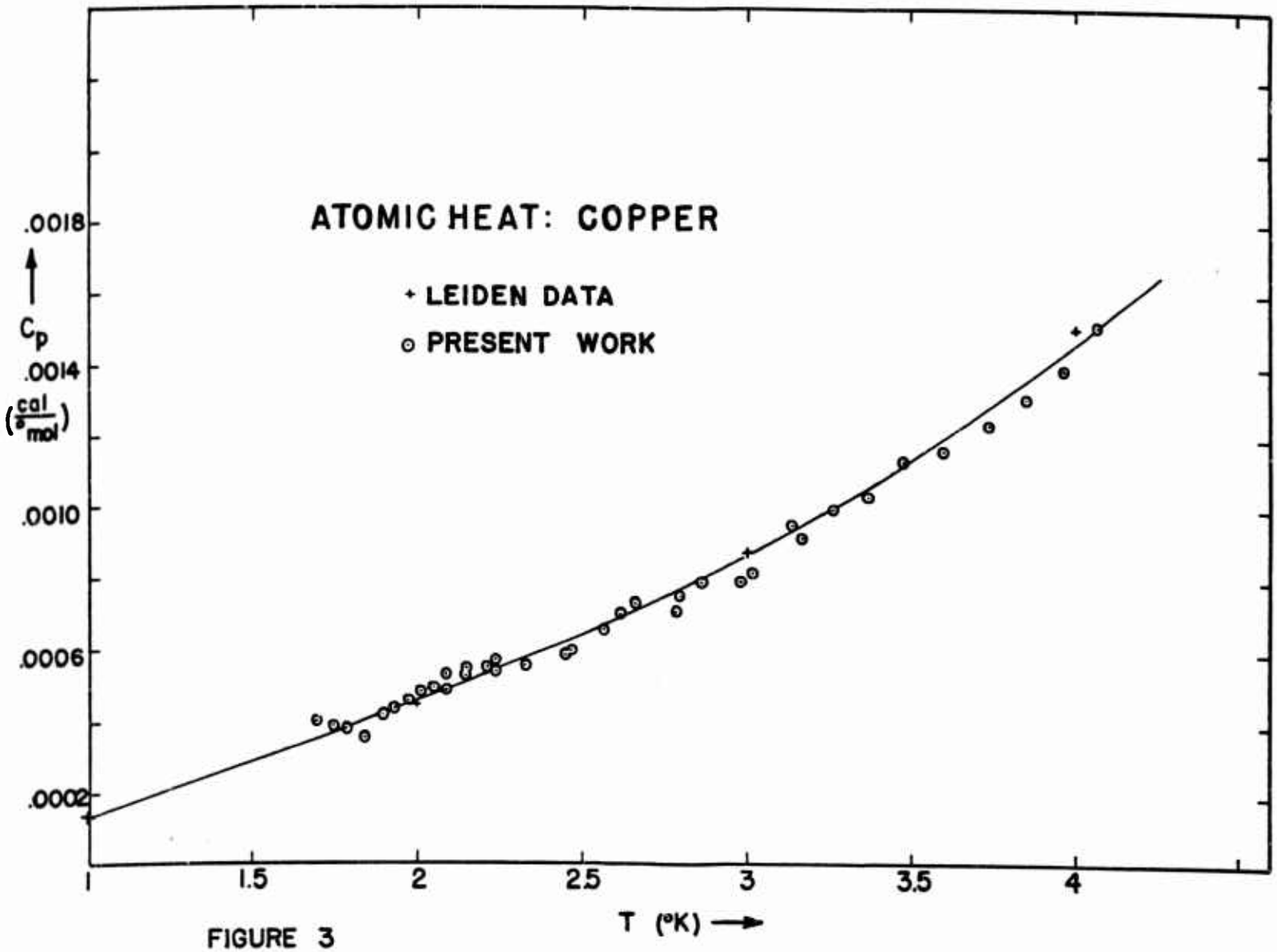
ATOMIC HEAT: COPPER
+ LEIDEN DATA
⊙ PRESENT WORK
.0018
.0014
.0010
.0006
.0002
C_p
$(\frac{cal}{°mol})$
1
1.5
2
2.5
3
3.5
4
T (°K) ⟶

FIGURE 3

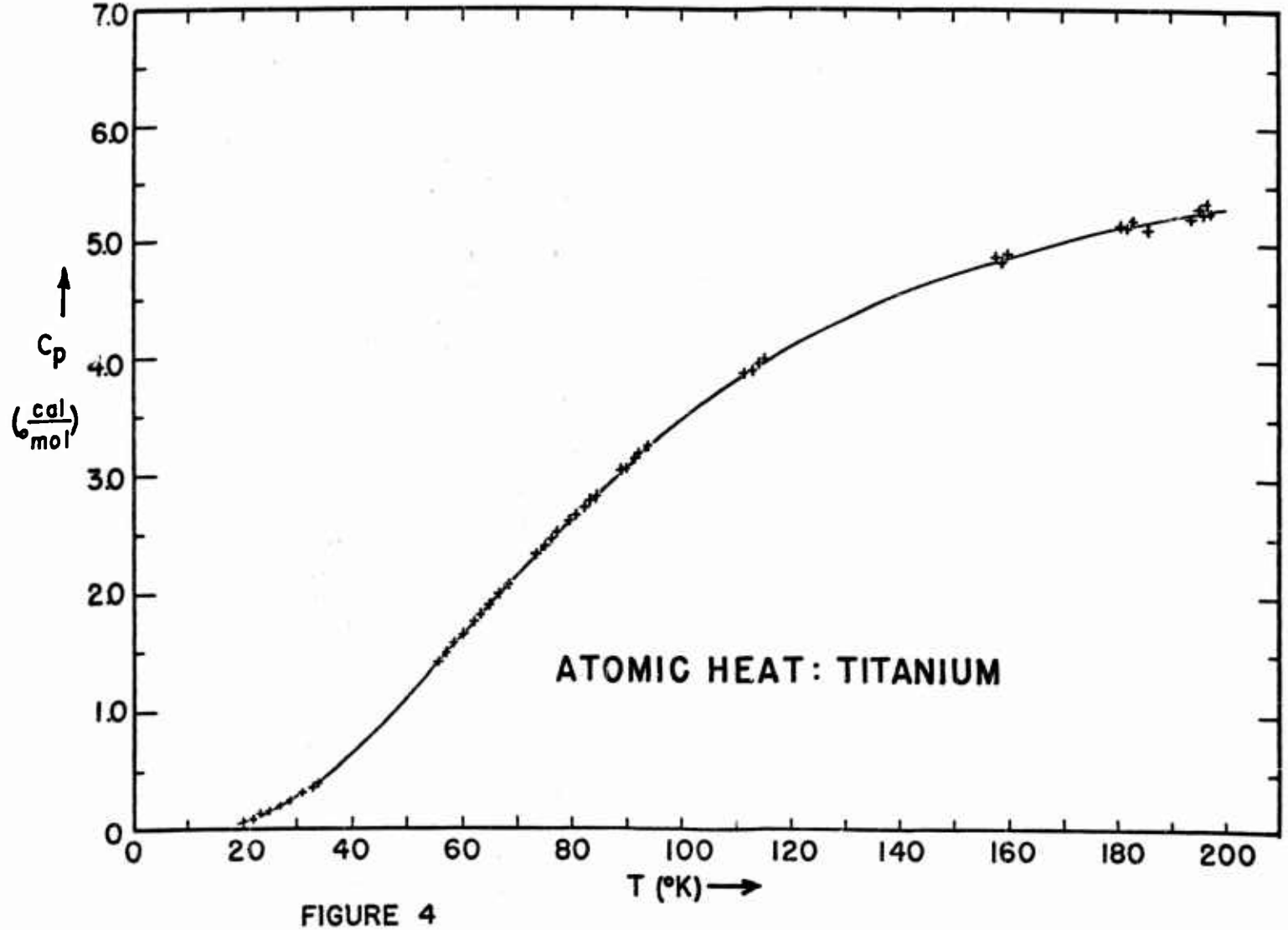
7.0
6.0
5.0
4.0
3.0
2.0
1.0
0
C_p
$(\frac{cal}{mol})$
ATOMIC HEAT: TITANIUM
0
20
40
60
80
100
120
140
160
180
200
T (°K) ⟶

FIGURE 4

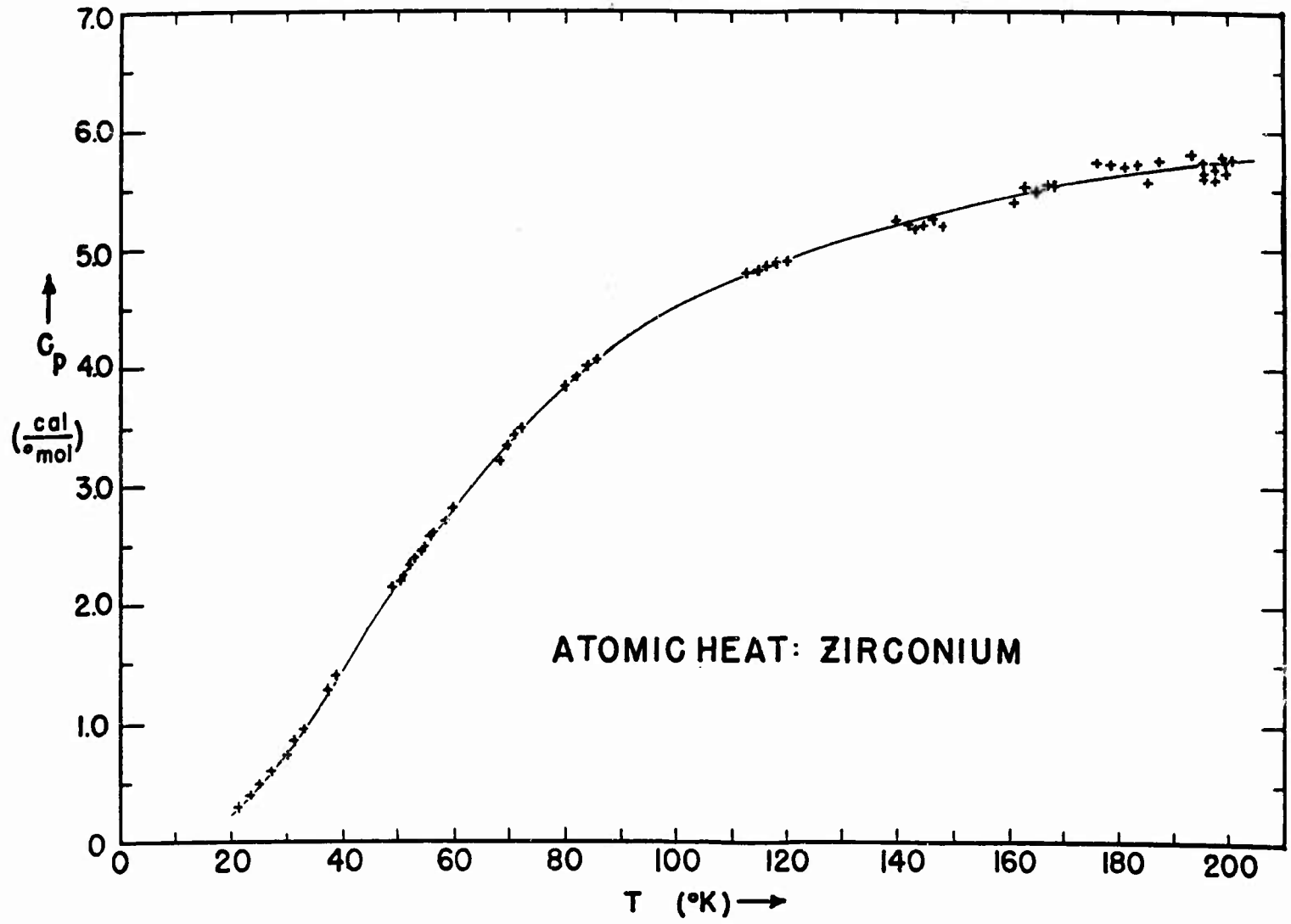
7.0
6.0
5.0
4.0
3.0
2.0
1.0
0
C_p
$(\frac{cal}{°mol})$
0
20
40
60
80
100
120
140
160
180
200
T (°K) ⟶
ATOMIC HEAT: ZIRCONIUM

FIGURE 5

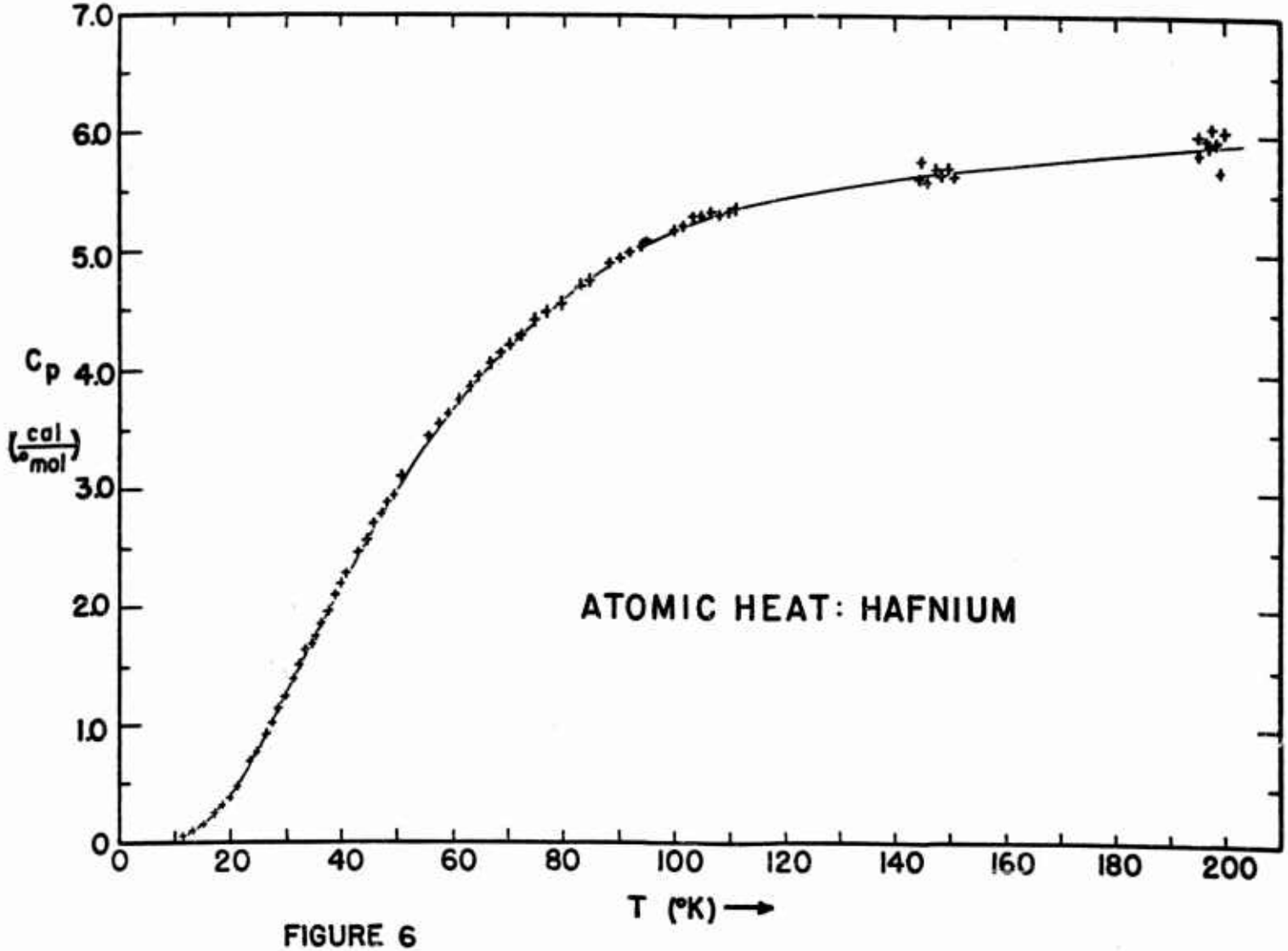
7.0
6.0
5.0
4.0
3.0
2.0
1.0
0
C_p
$\left(\frac{cal}{°mol}\right)$
ATOMIC HEAT: HAFNIUM
0
20
40
60
80
100
120
140
160
180
200
T (°K) ⟶

FIGURE 6

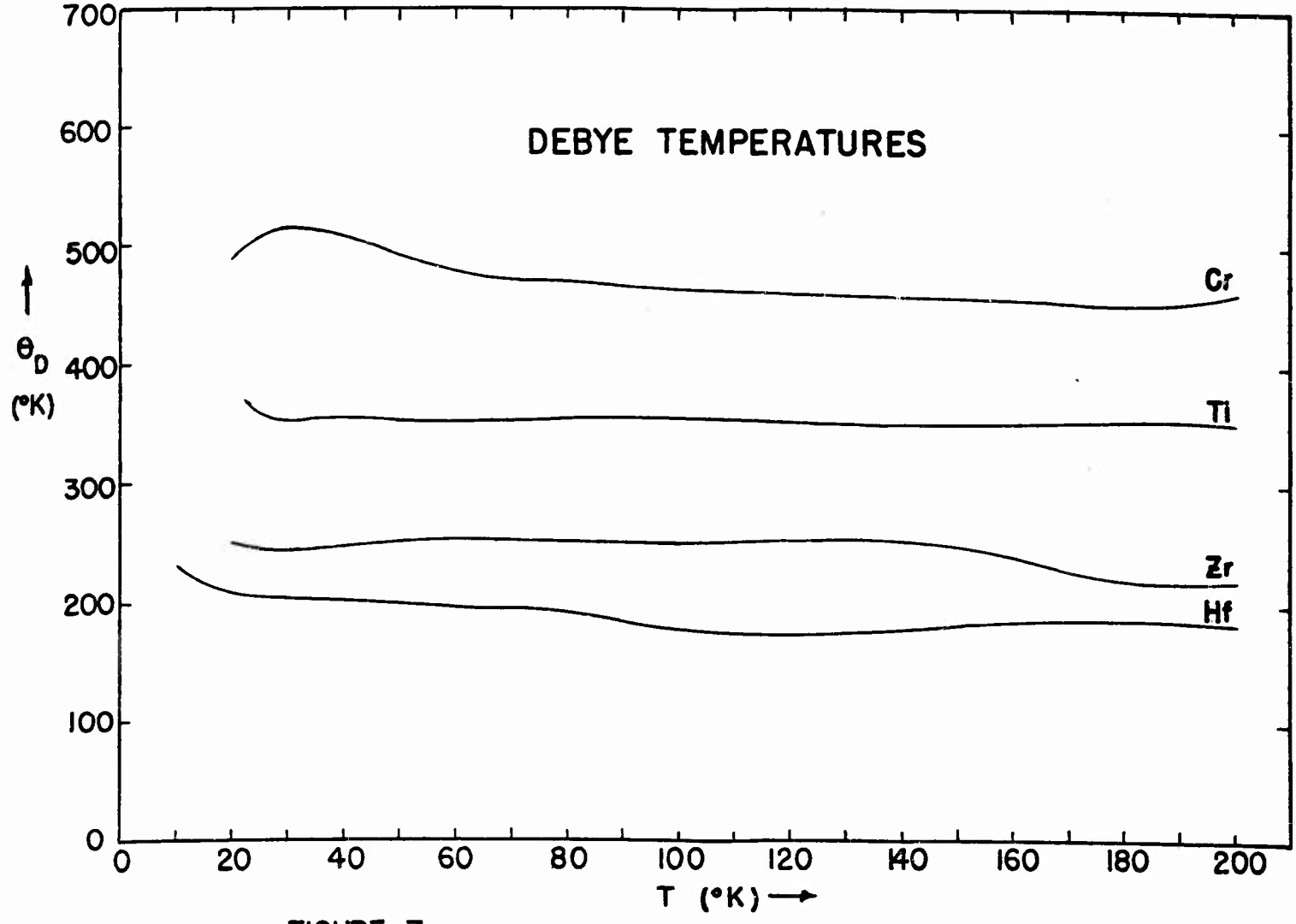
DEBYE TEMPERATURES
700
600
500
400
300
200
100
0
θ_D (°K)
Cr
Ti
Zr
Hf
0
20
40
60
80
100
120
140
160
180
200
T (°K) →

FIGURE 7

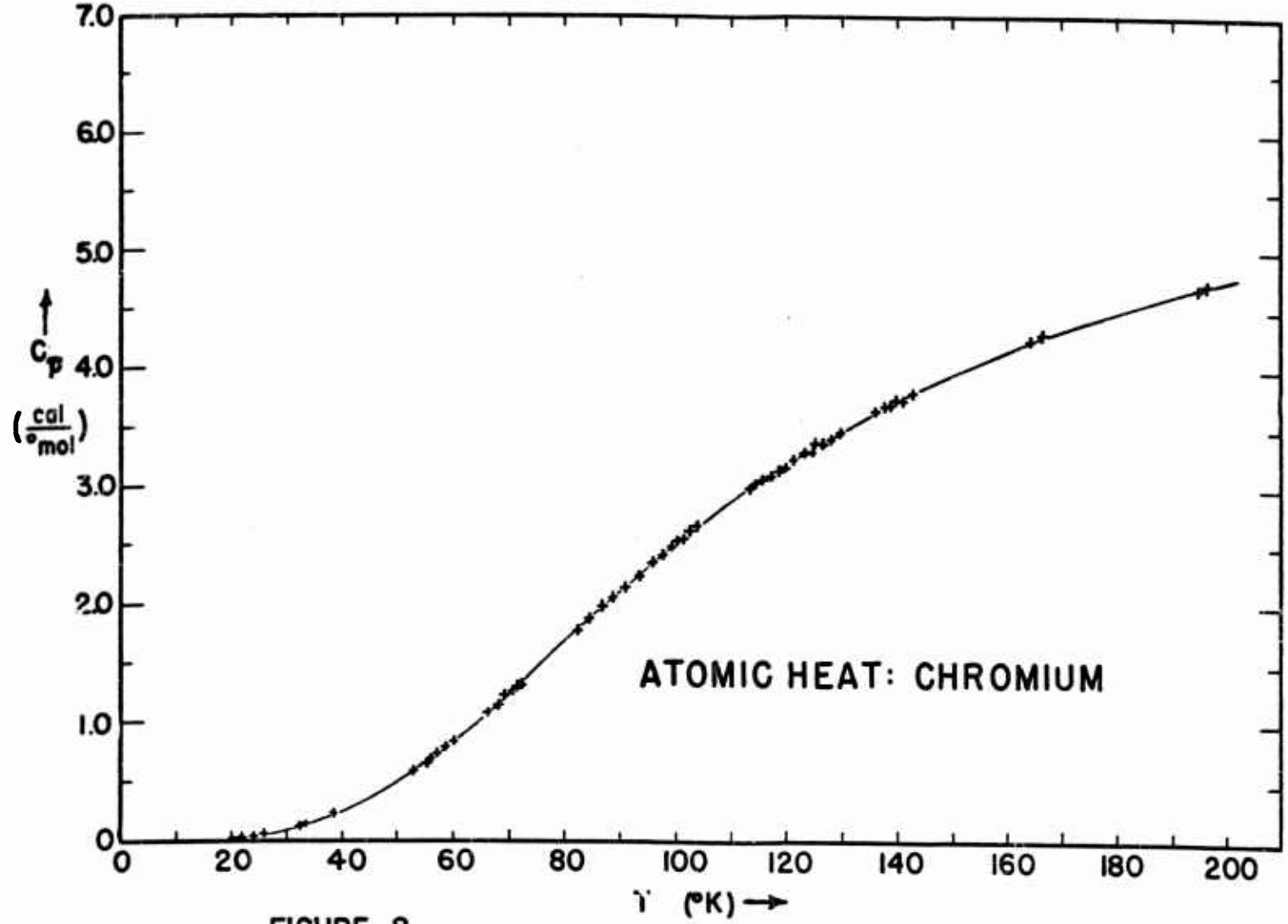
7.0
6.0
5.0
4.0
3.0
2.0
1.0
0
C_p
$(\frac{cal}{°mol})$
0
20
40
60
80
100
120
140
160
180
200
T (°K) →
ATOMIC HEAT: CHROMIUM

FIGURE 8

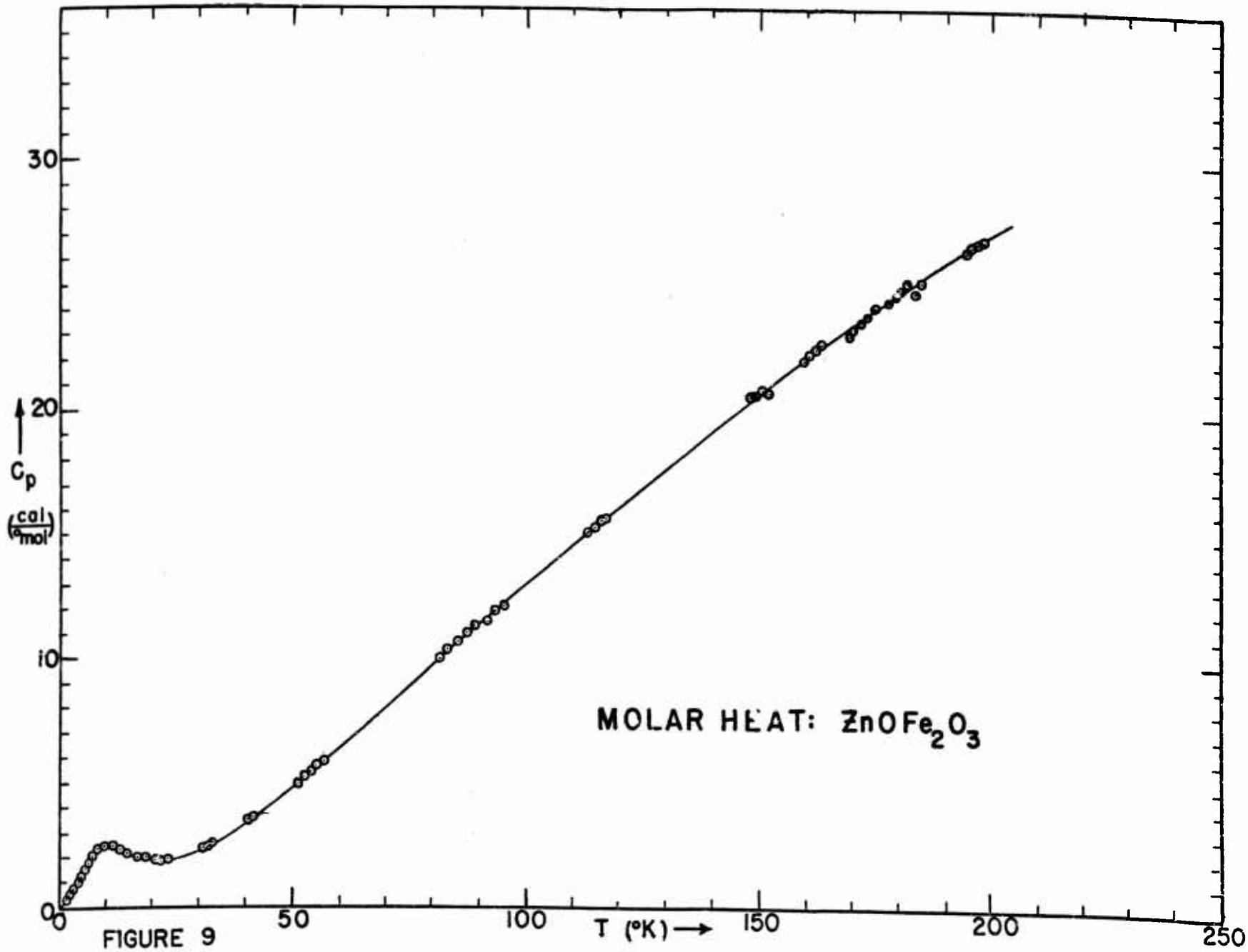
30
20
10
0
C_p
$\left(\frac{cal}{°mol}\right)$
0
50
100
150
200
250
T (°K) →
MOLAR HEAT: $ZnOFe_2O_3$

FIGURE 9

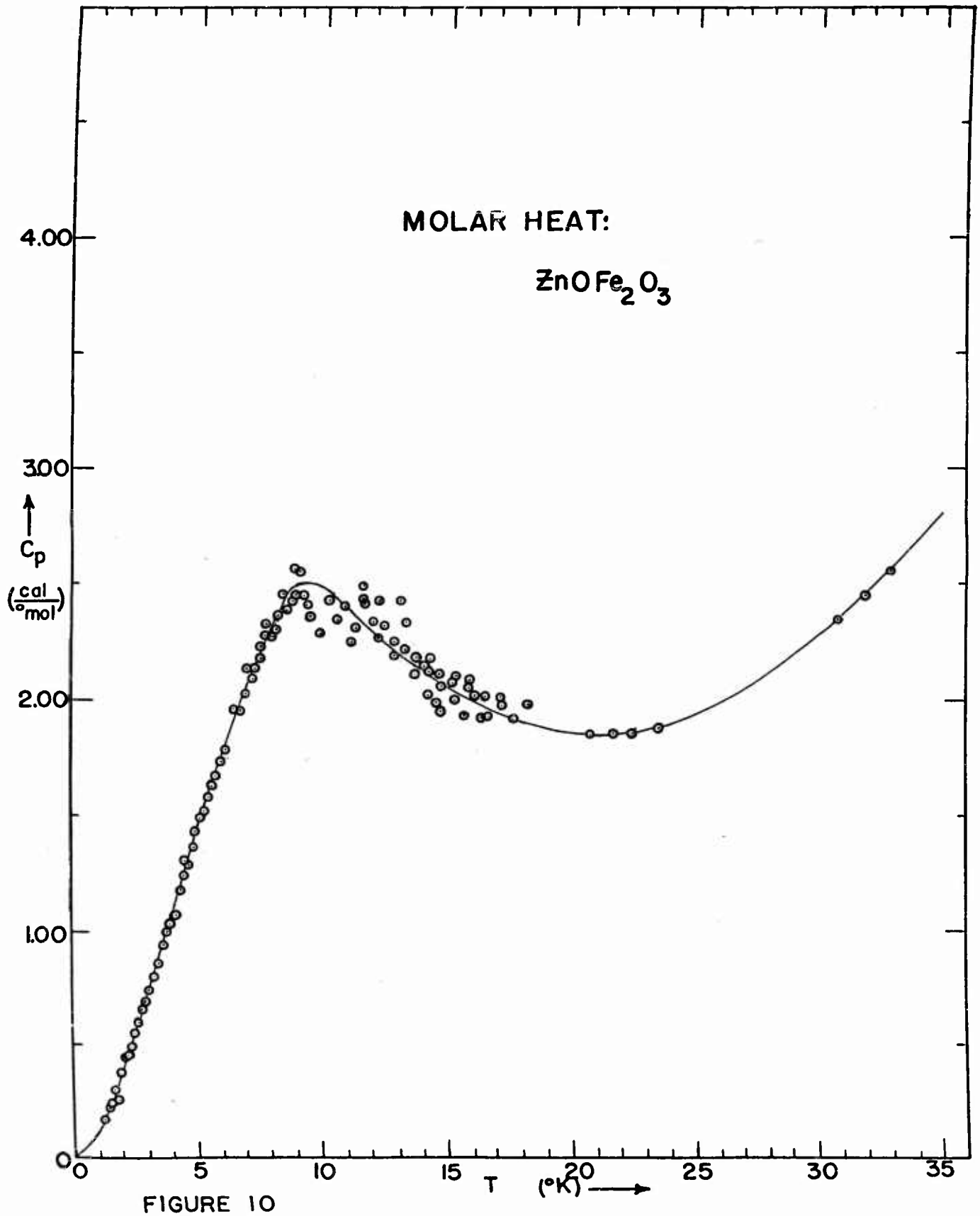
MOLAR HEAT:
ZnO Fe2 O3
4.00
3.00
2.00
1.00
0
Cp
(cal/°mol)
0
5
10
15
20
25
30
35
T (°K) ⟶

FIGURE 10

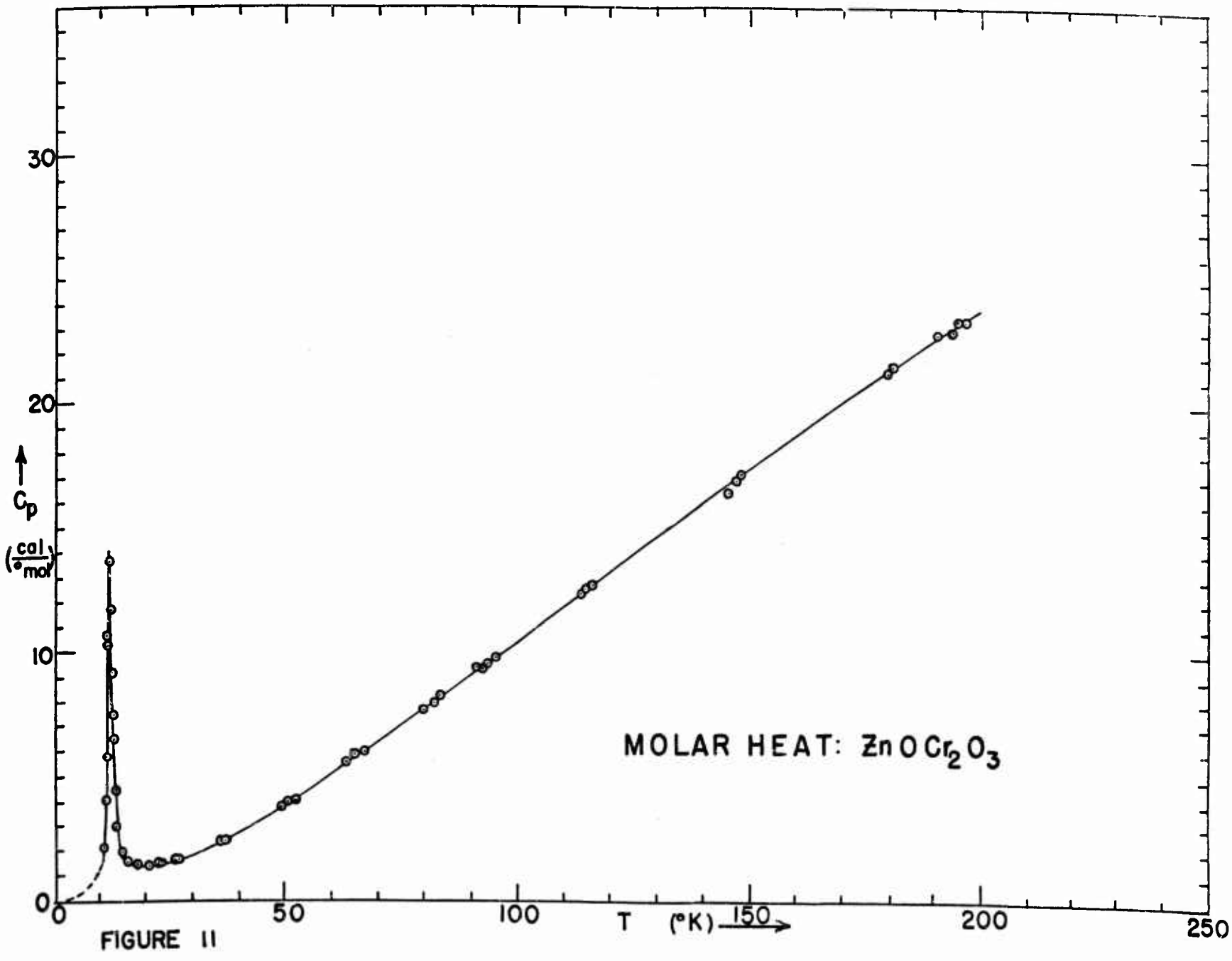
30
20
10
0
C_p
$\left(\frac{cal}{°mol}\right)$
0
50
100
T (°K) 150
200
250
MOLAR HEAT: $ZnOCr_2O_3$

FIGURE 11

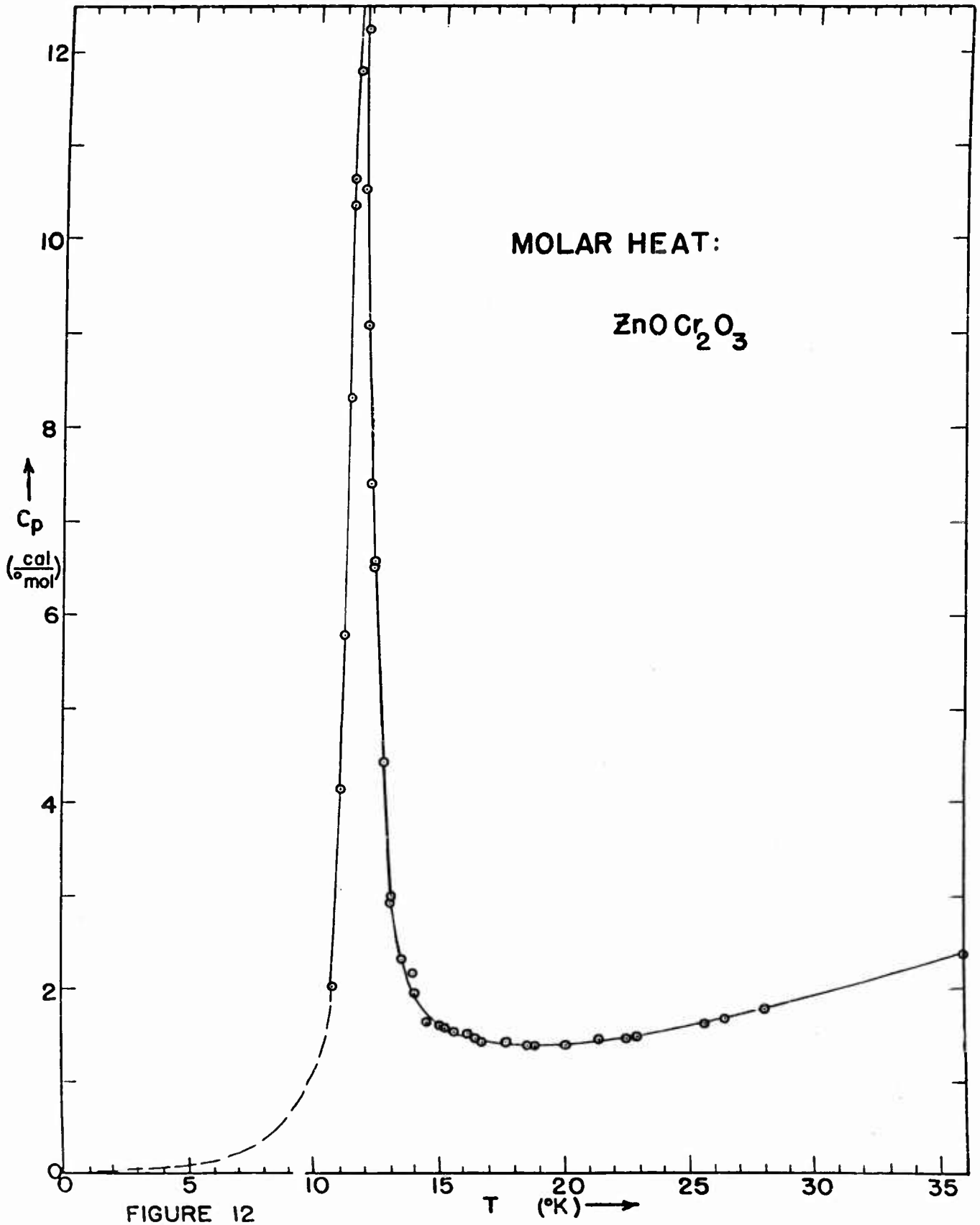

FIGURE 12

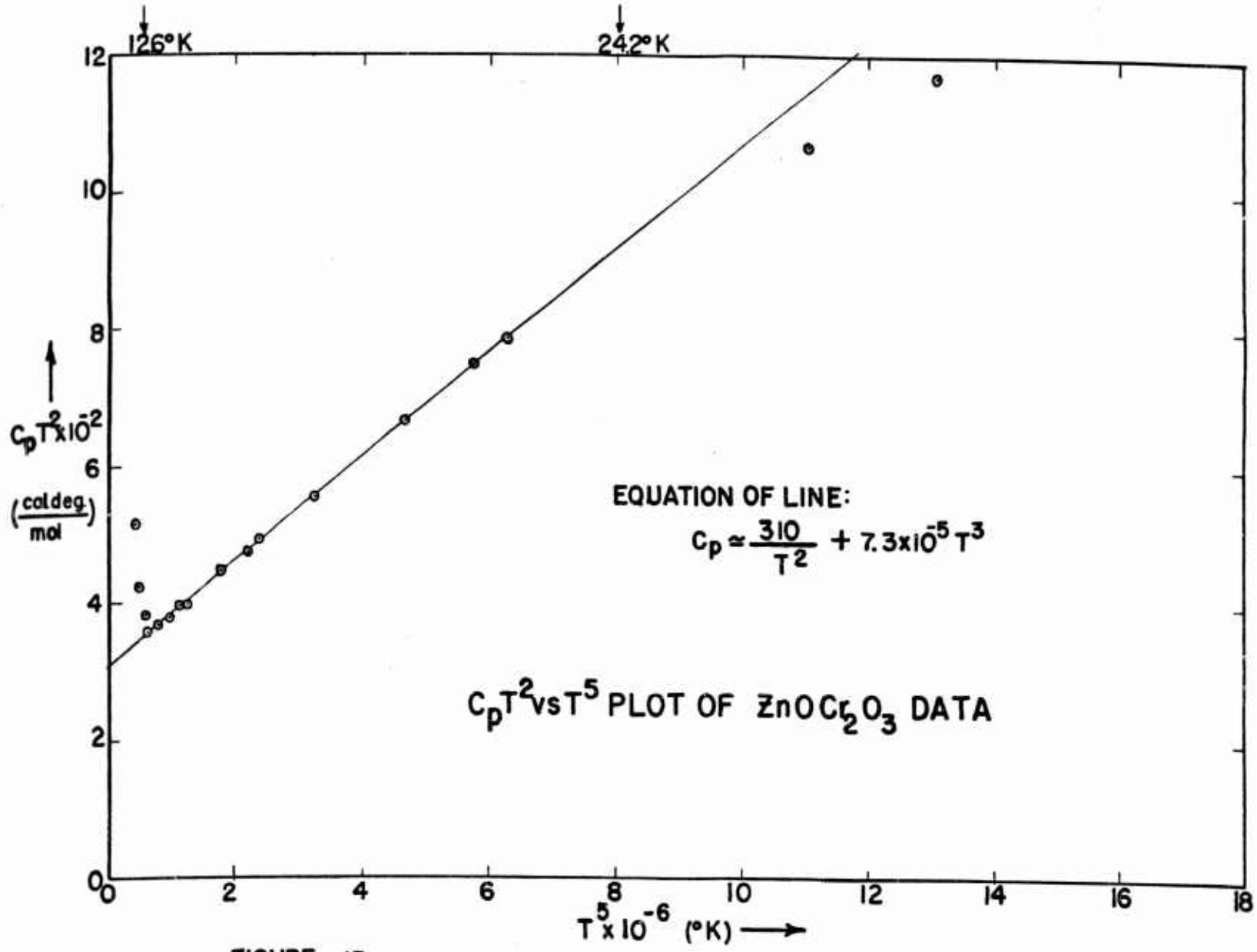
12.6°K
24.2°K
12
10
8
6
4
2
0
$C_pT^2 \times 10^{-2}$
$\left(\frac{\text{cal deg}}{\text{mol}}\right)$
EQUATION OF LINE:
$C_p \simeq \frac{310}{T^2} + 7.3 \times 10^{-5} T^3$
C_pT^2 vs T^5 PLOT OF $ZnOCr_2O_3$ DATA
0
2
4
6
8
10
12
14
16
18
$T^5 \times 10^{-6}$ (°K) ⟶

FIGURE 13

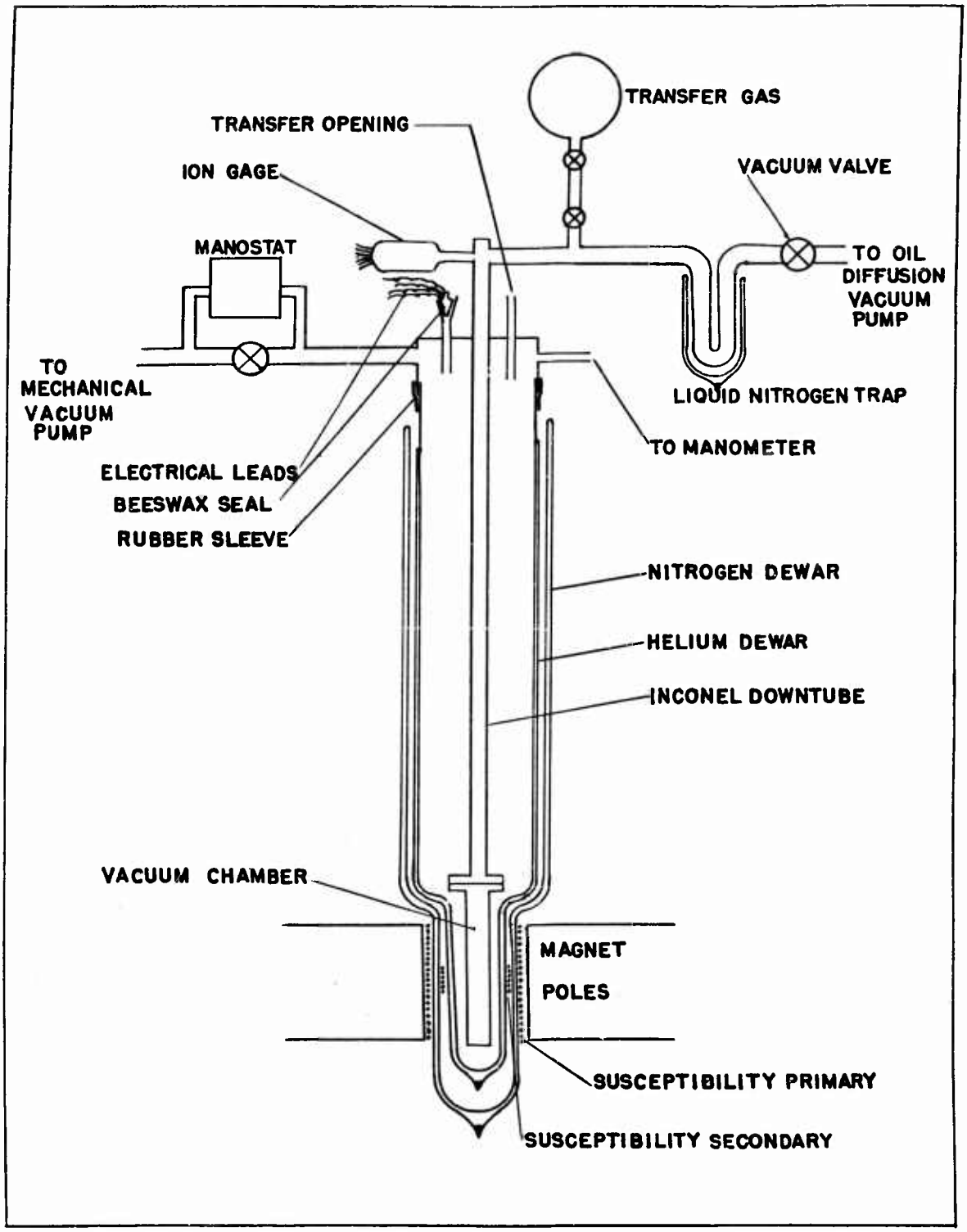

FIGURE 14 CRYOSTAT FOR MEASUREMENTS BELOW 1.3°K-SCHEMATIC

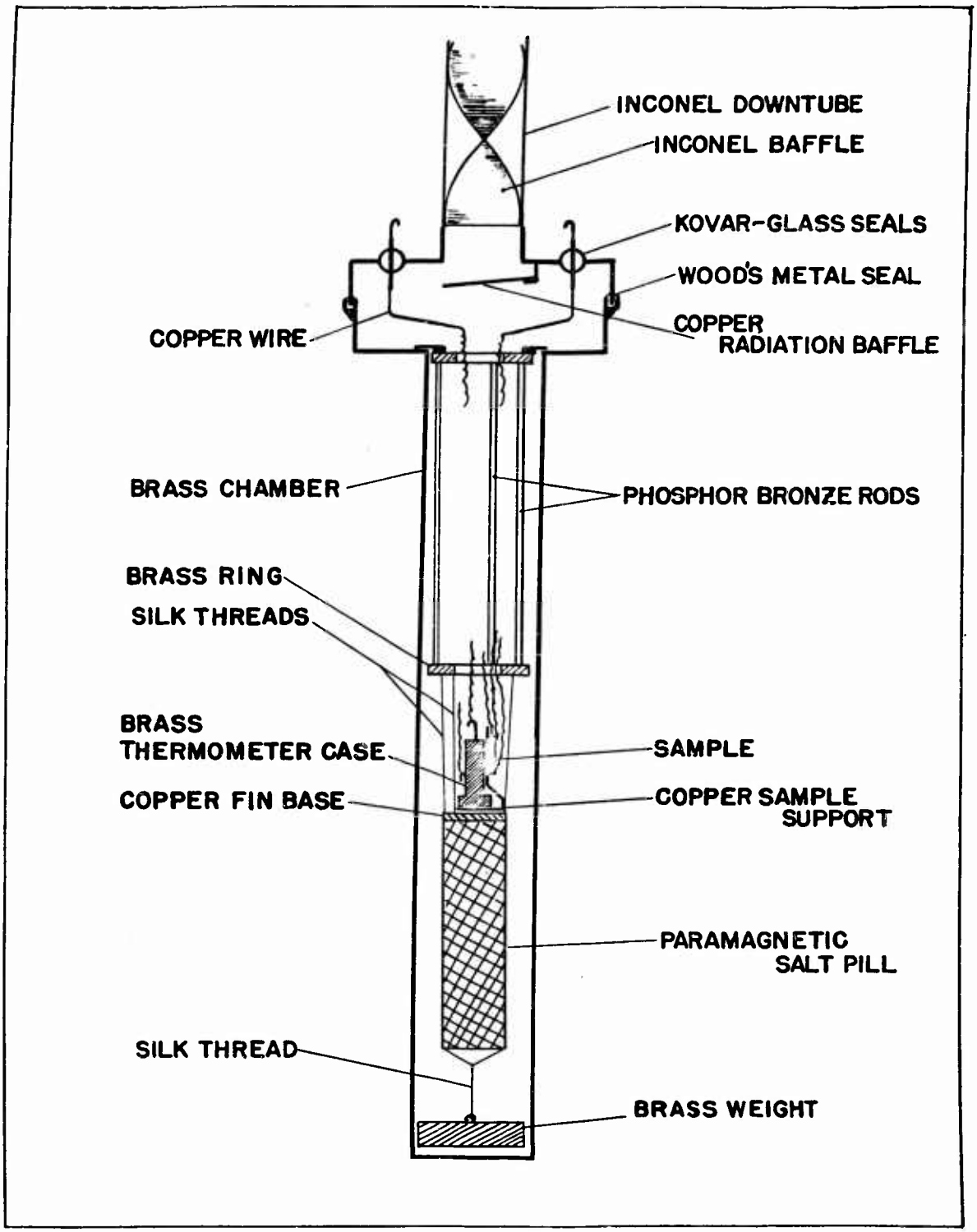

FIGURE 15 CRYOSTAT VACUUM CHAMBER - CROSS SECTION

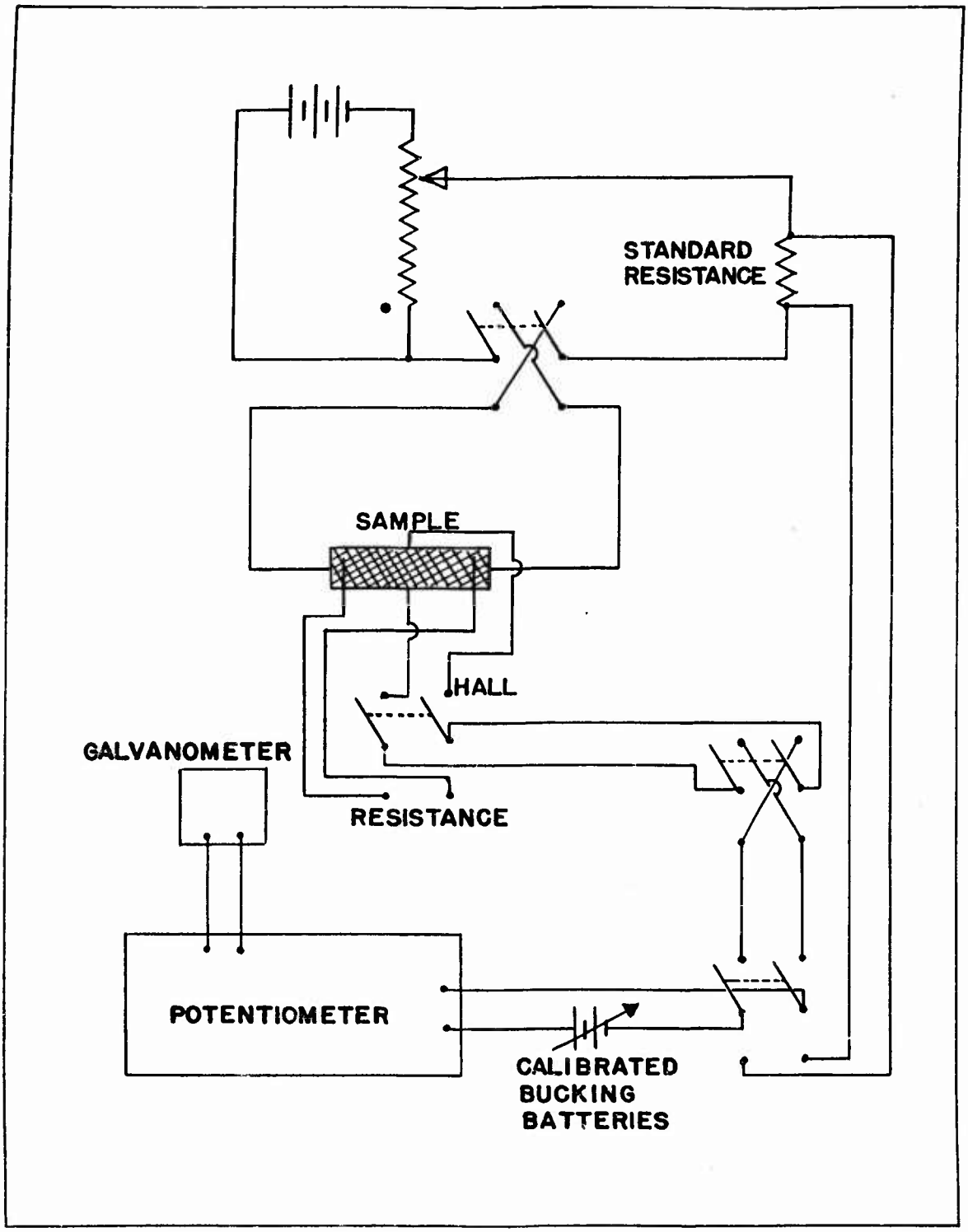

FIGURE 16 CIRCUIT FOR ELECTRICAL MEASURMENTS

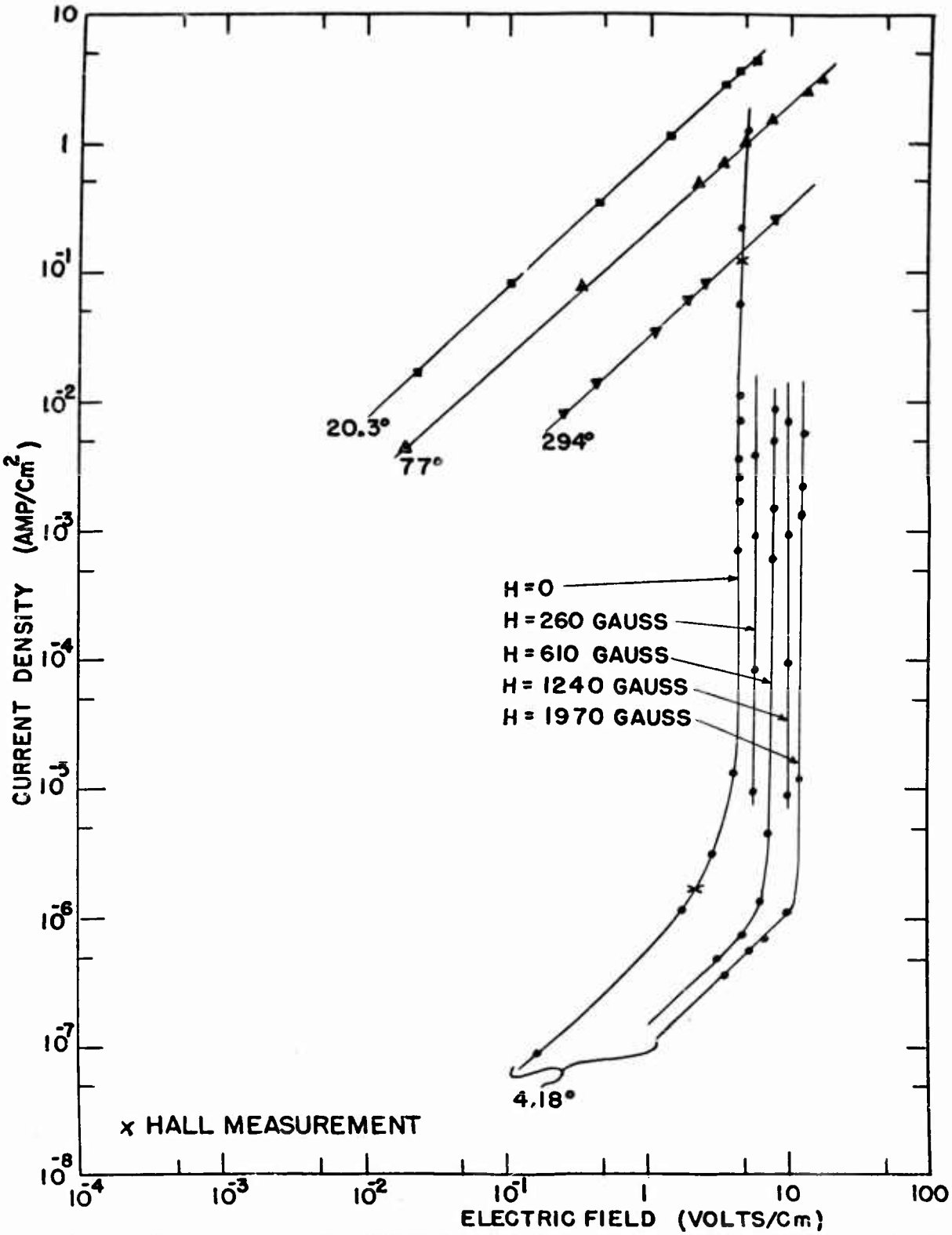

FIGURE 17 CURRENT DENSITY vs ELECTRIC FIELD FOR B42

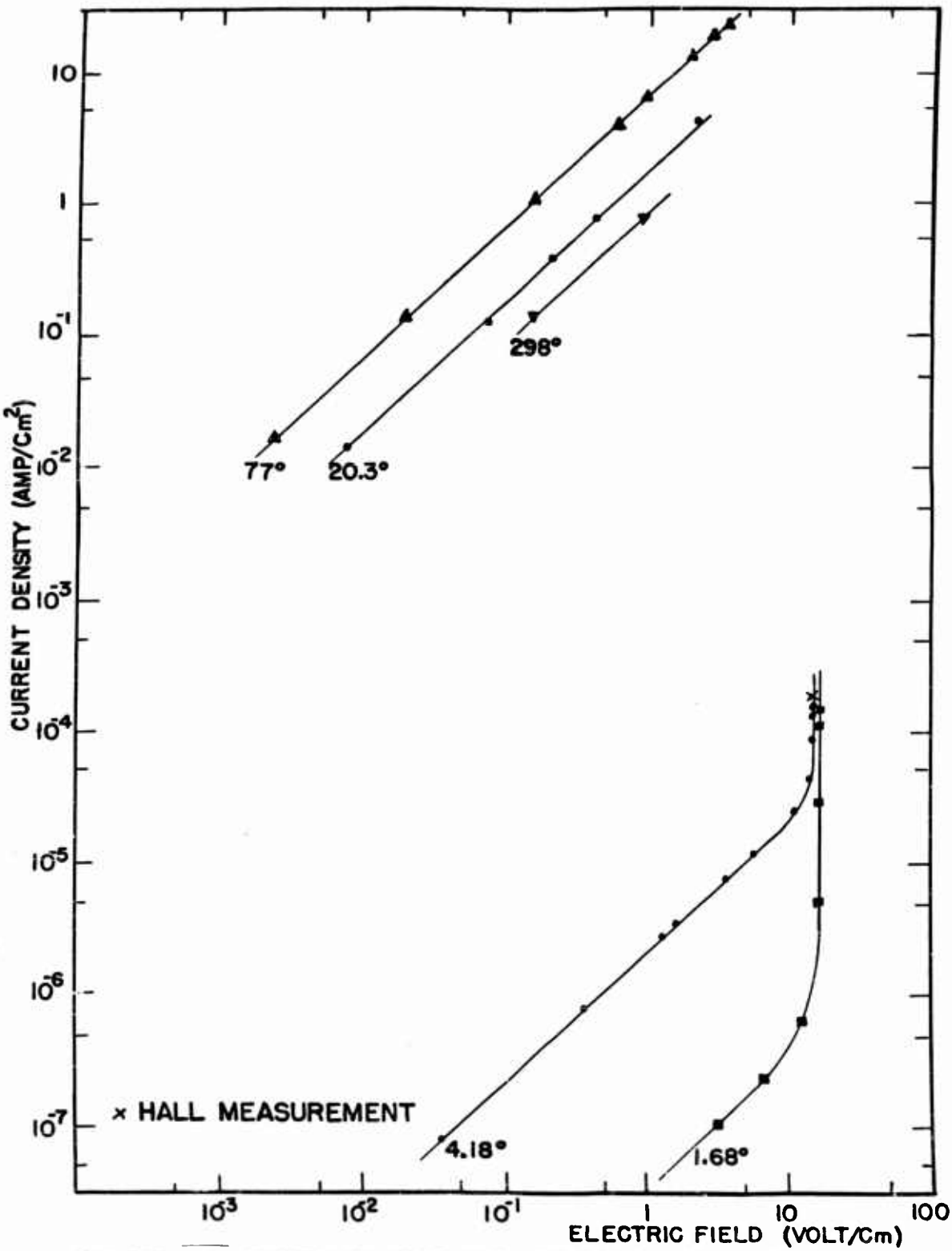

FIGURE 18 CURRENT DENSITY vs ELECTRIC FIELD FOR B12

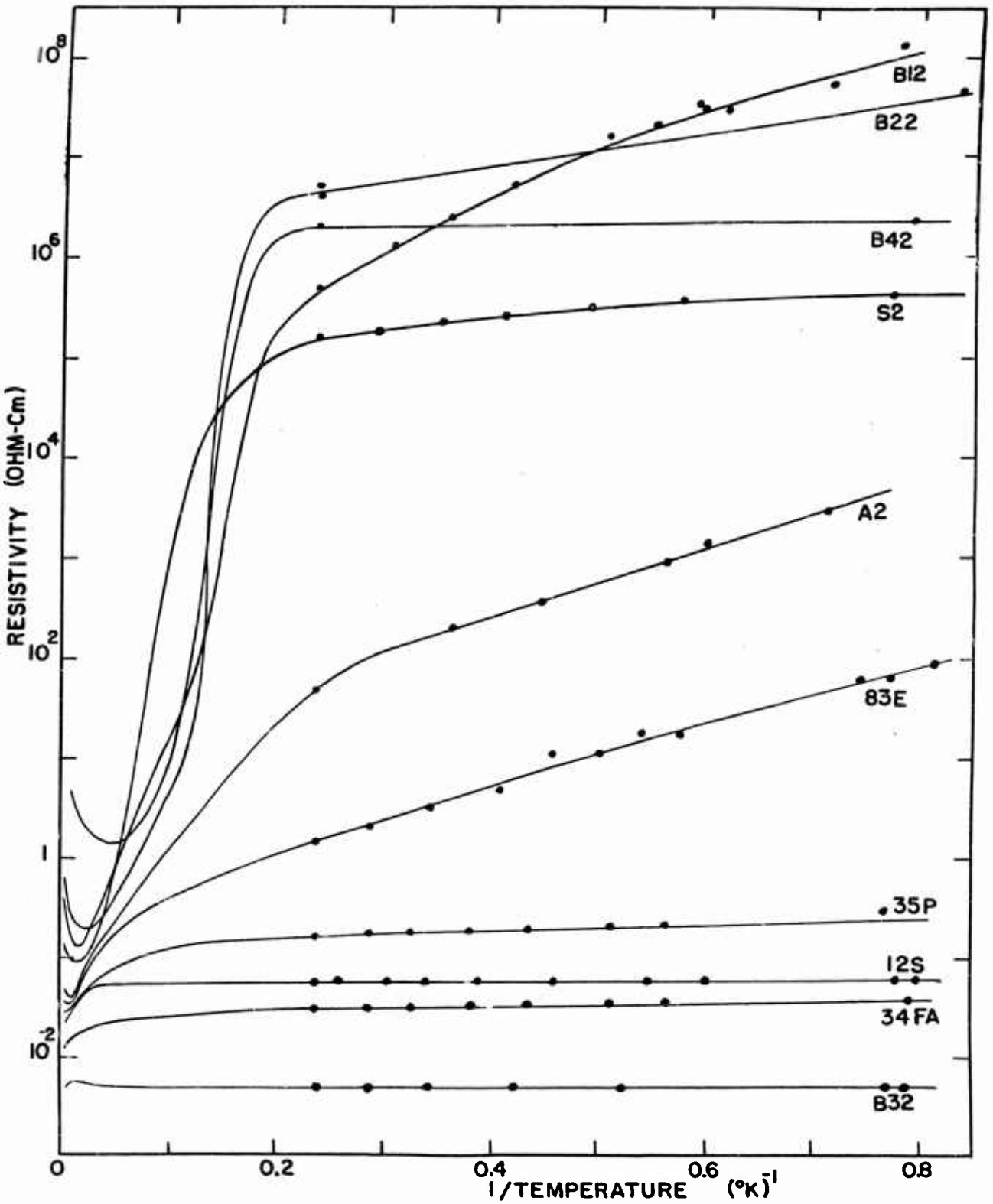

FIGURE 19 RESISTIVITY vs 1/TEMPERATURE FOR GERMANIUM SAMPLES

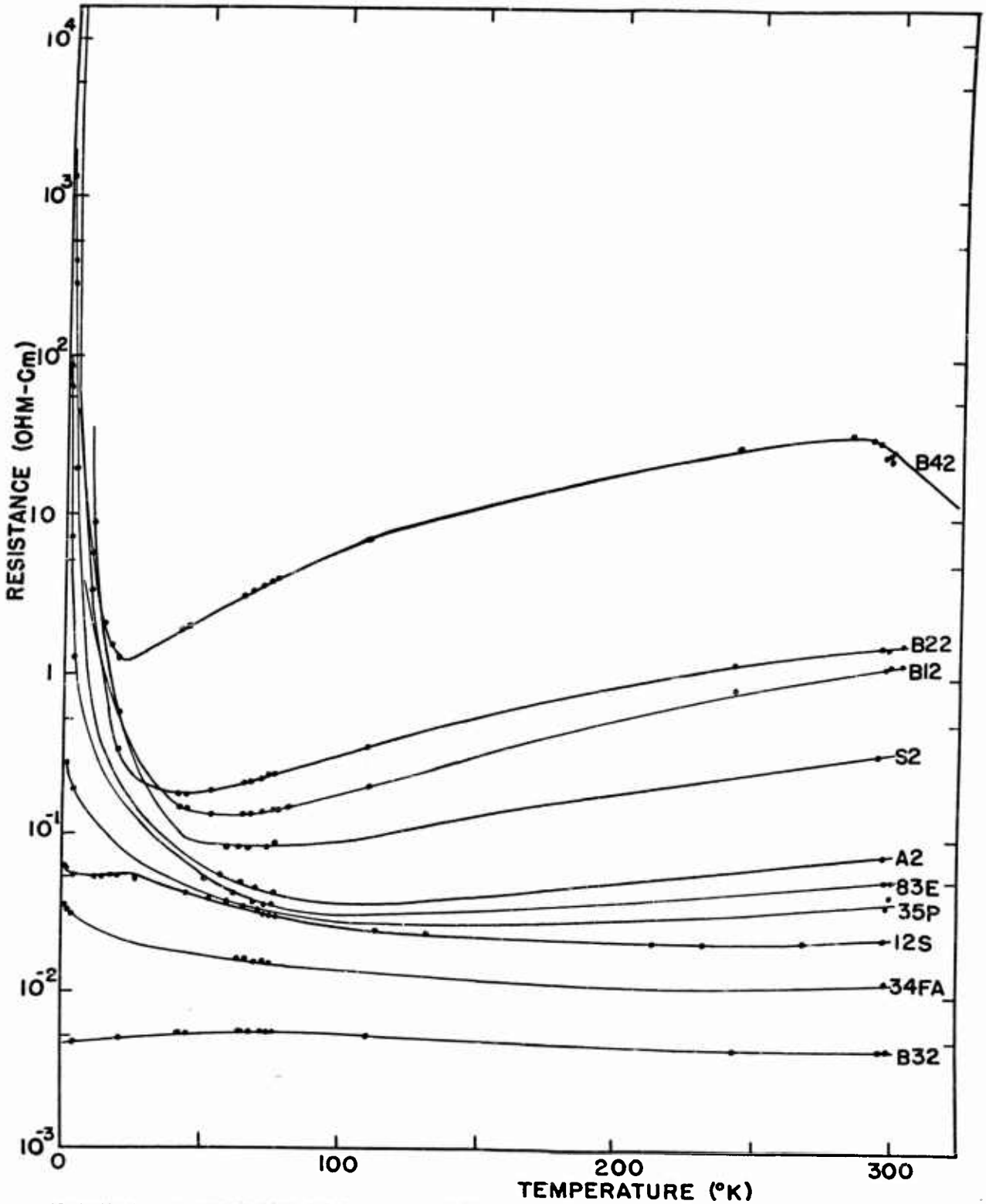

FIGURE 20 RESISTIVITY vs TEMPERATURE FOR GERMANIUM SAMPLES

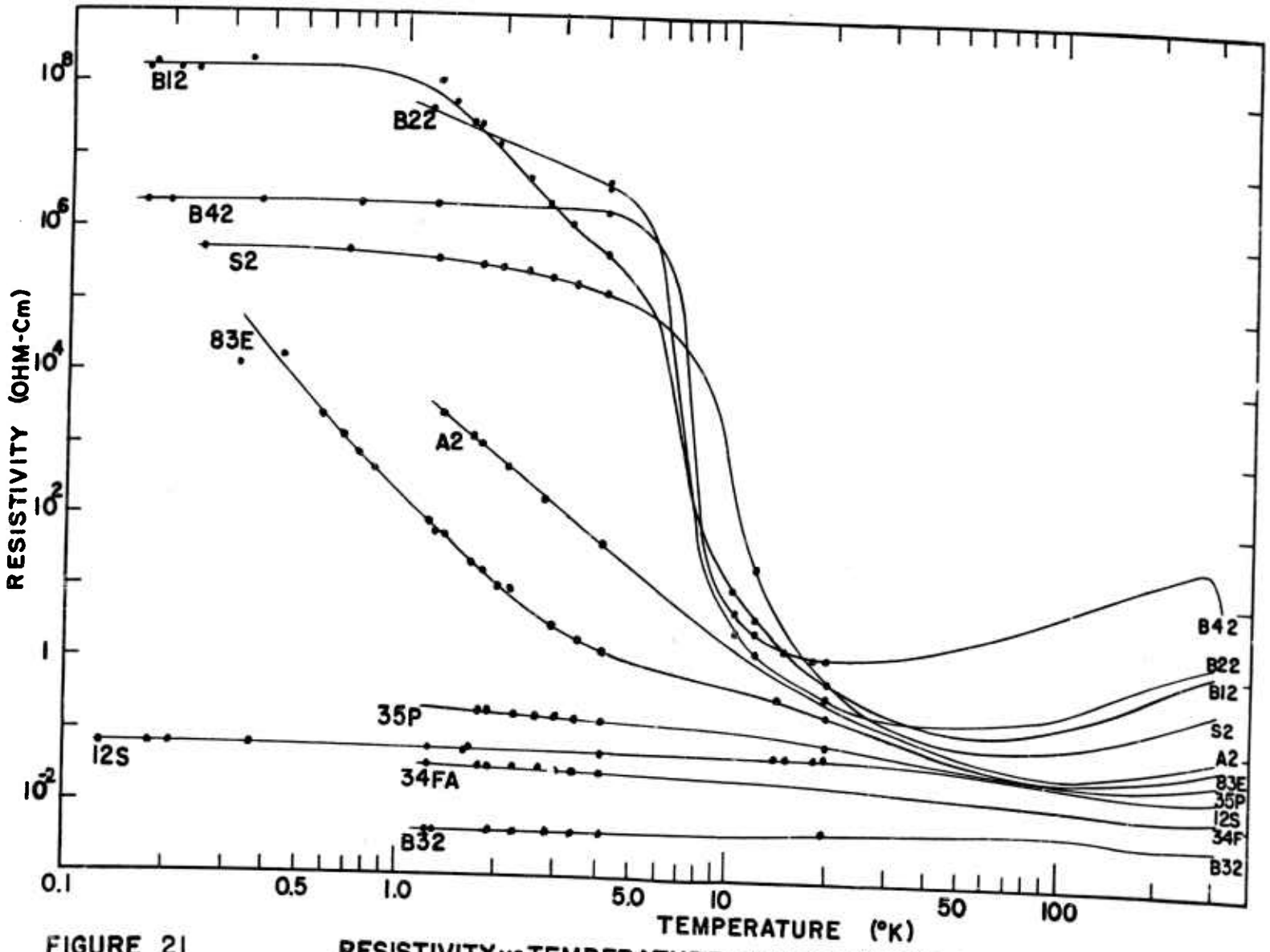

FIGURE 21 RESISTIVITY vs TEMPERATURE FOR GERMANIUM SAMPLES

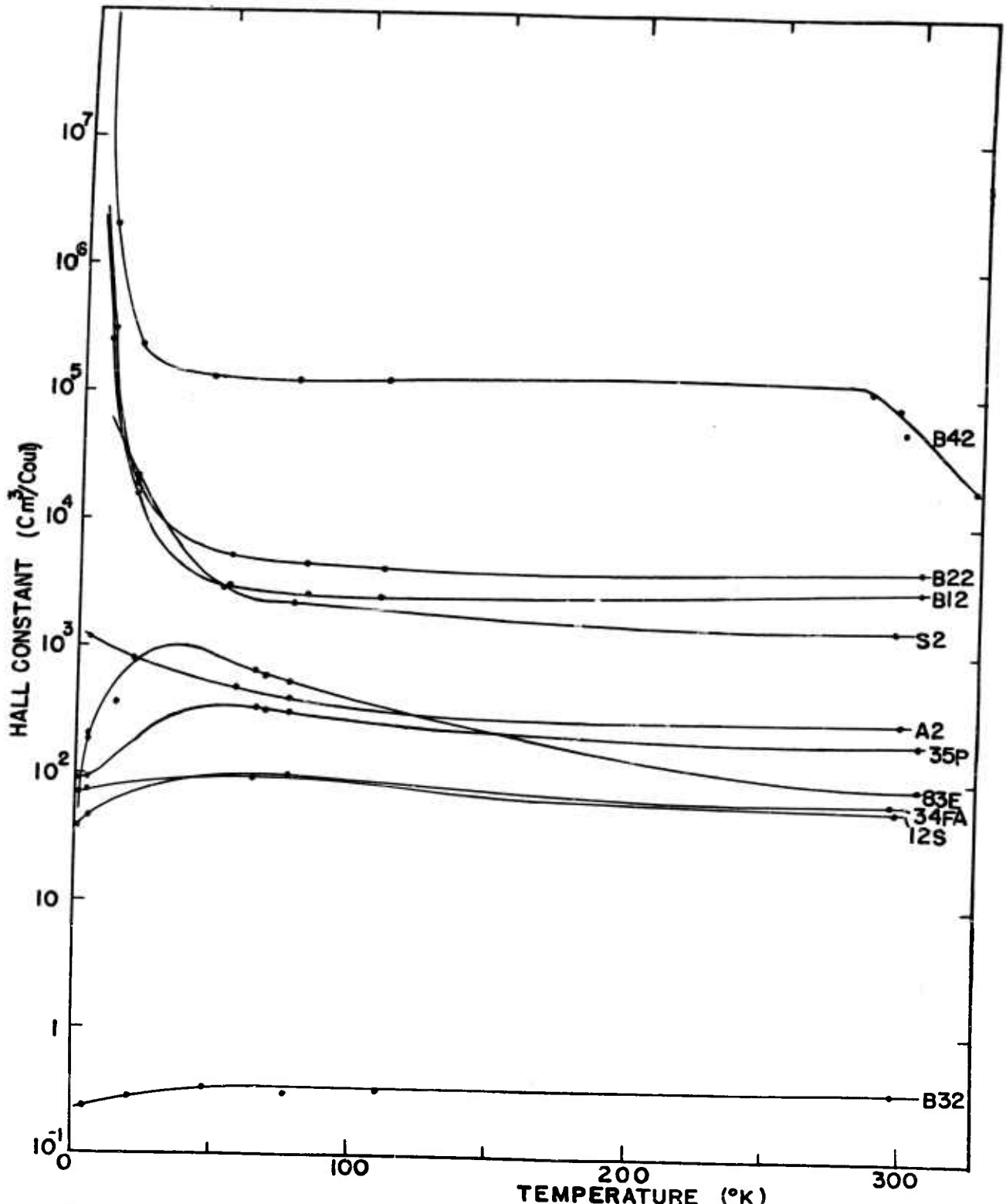

FIGURE 22 HALL CONSTANT vs TEMPERATURE FOR GERMANIUM SAMPLES

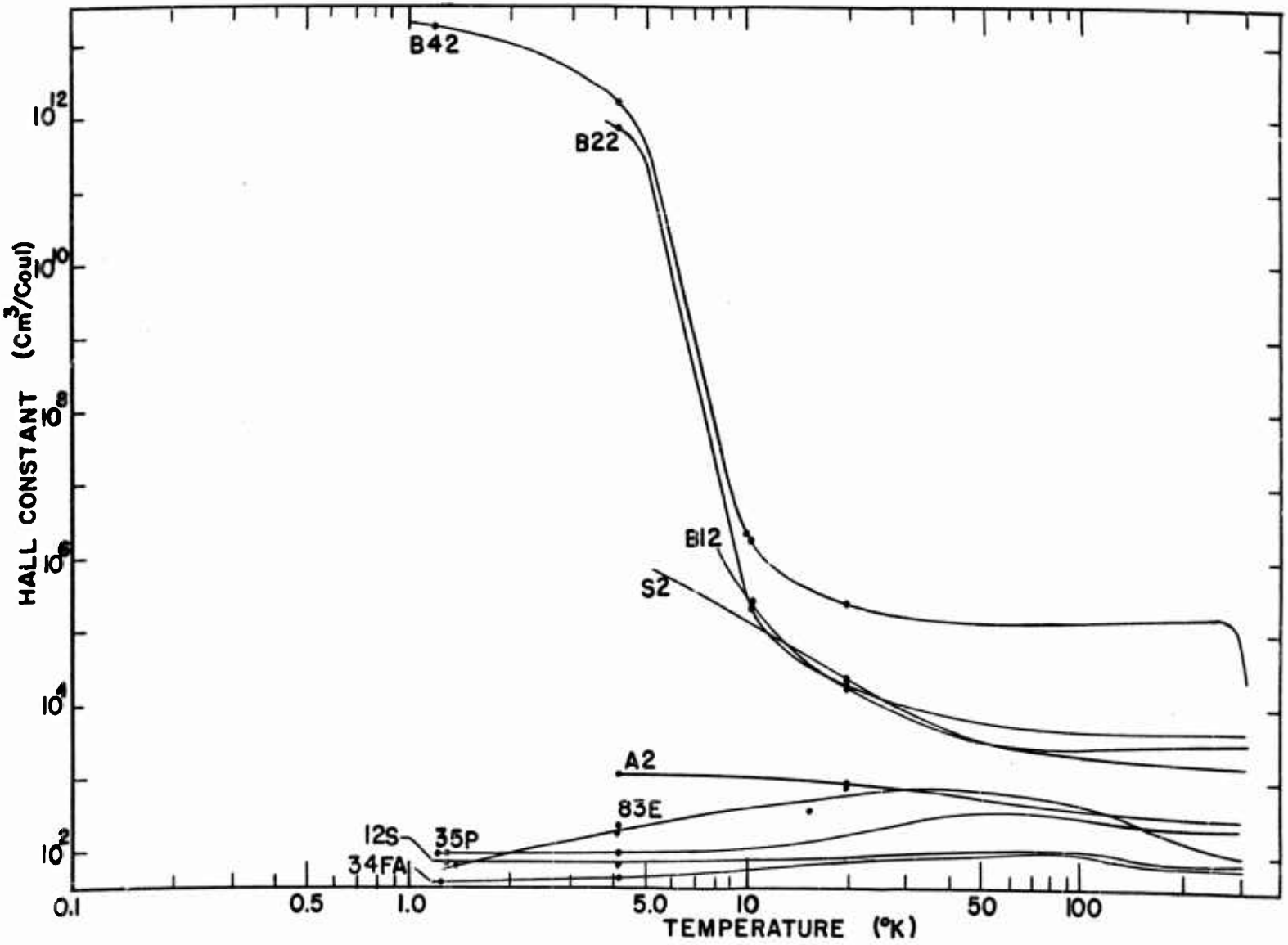

FIGURE 23 HALL CONSTANT vs TEMPERATURE FOR GERMANIUM SAMPLES

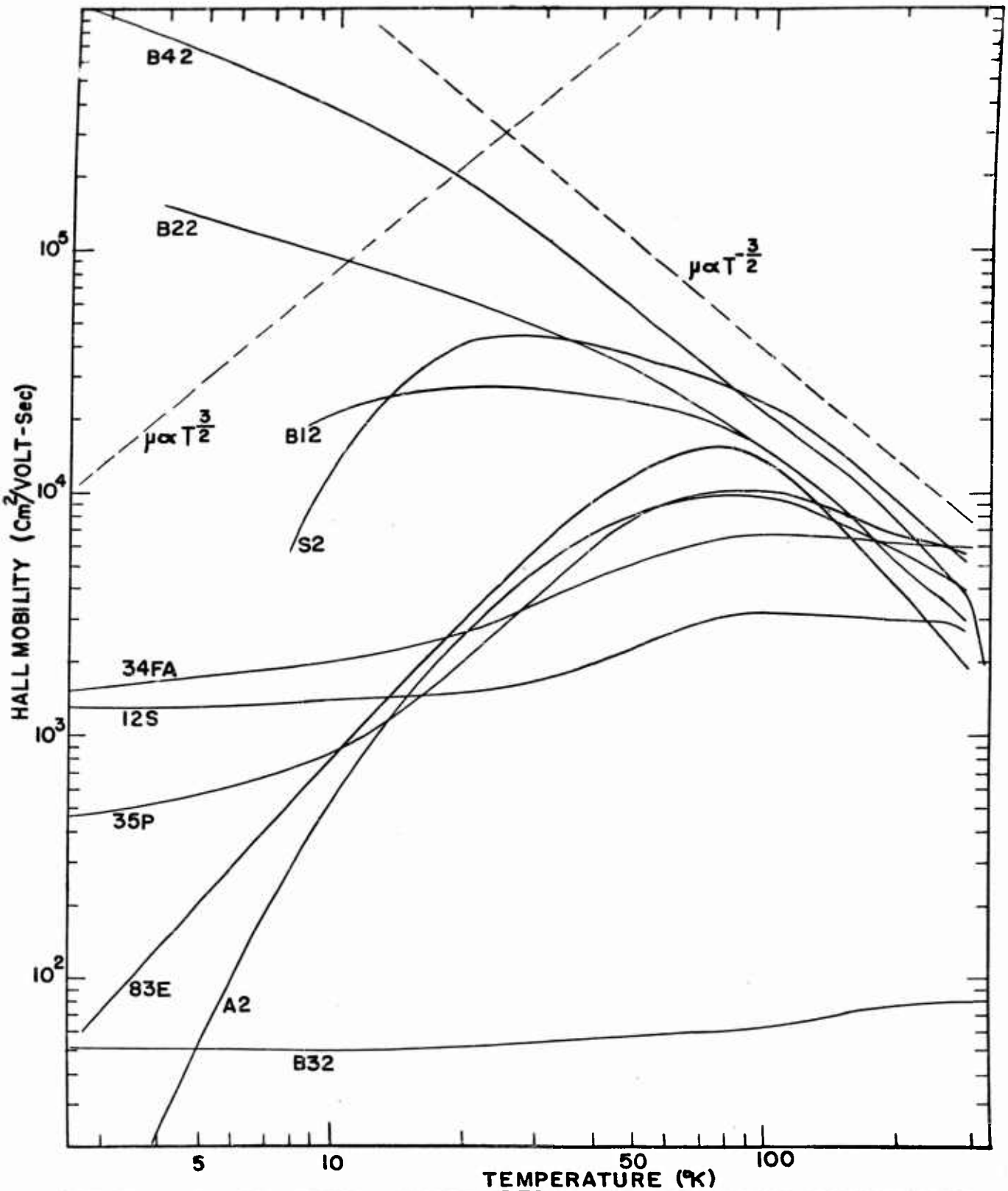

FIGURE 24 HALL MOBILITY vs TEMPERATURE FOR GERMANIUM SAMPLES

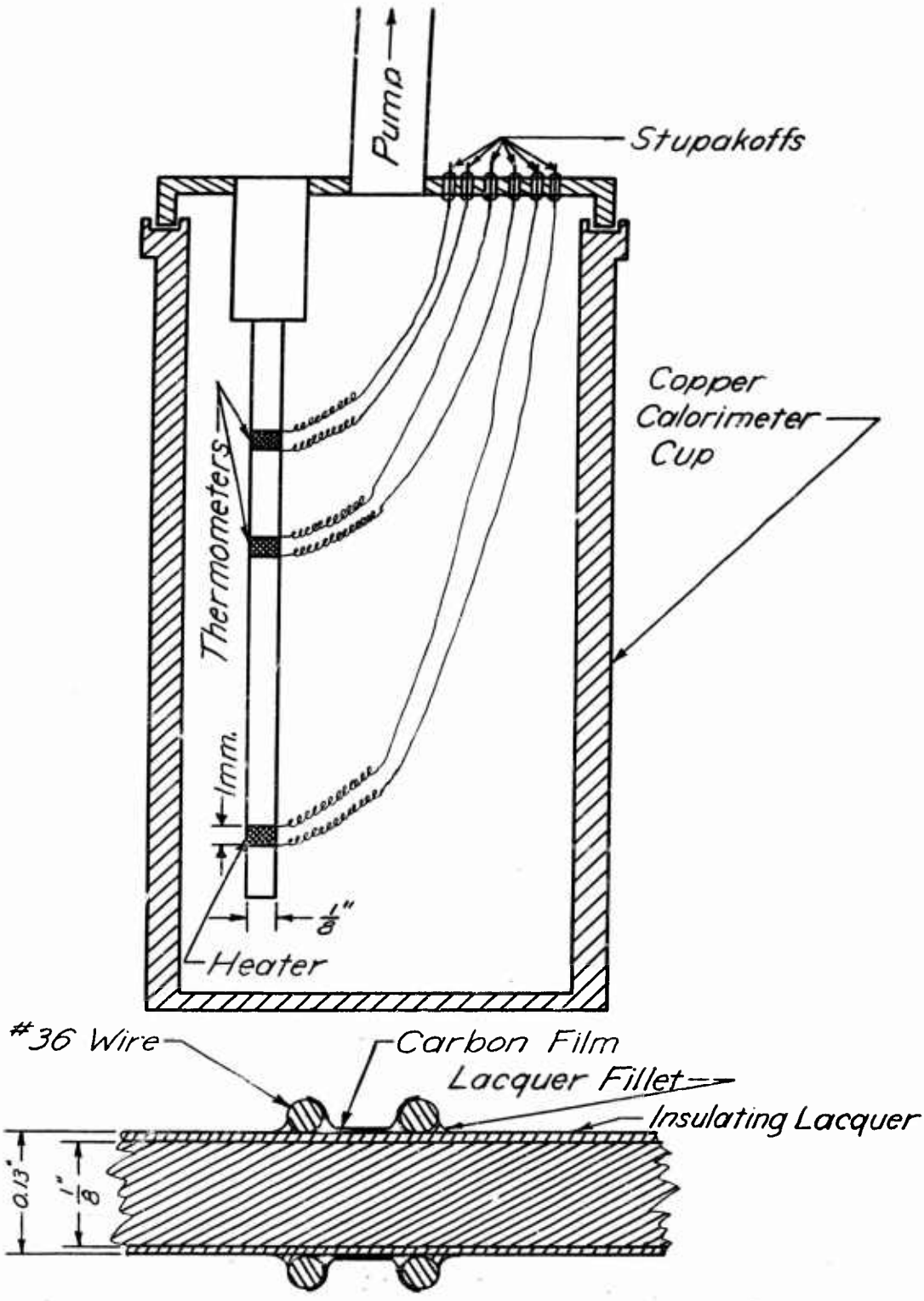

Thermometer Detail

FIGURE 25

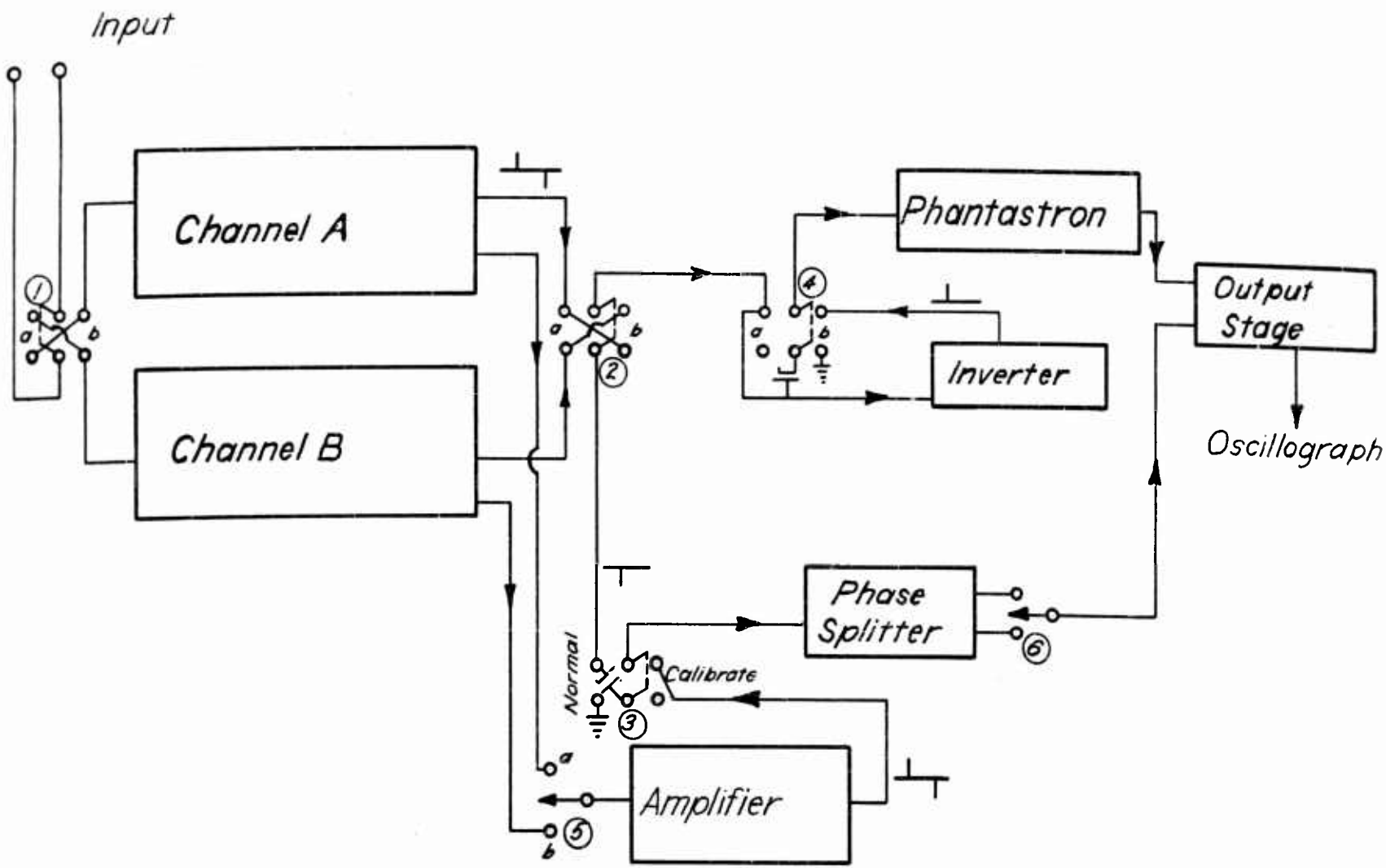
Input
Channel A
Channel B
Phantastron
Output Stage
Inverter
Oscillograph
Phase Splitter
Normal
Calibrate
Amplifier
1
2
3
4
5
6
a
b

FIGURE 26

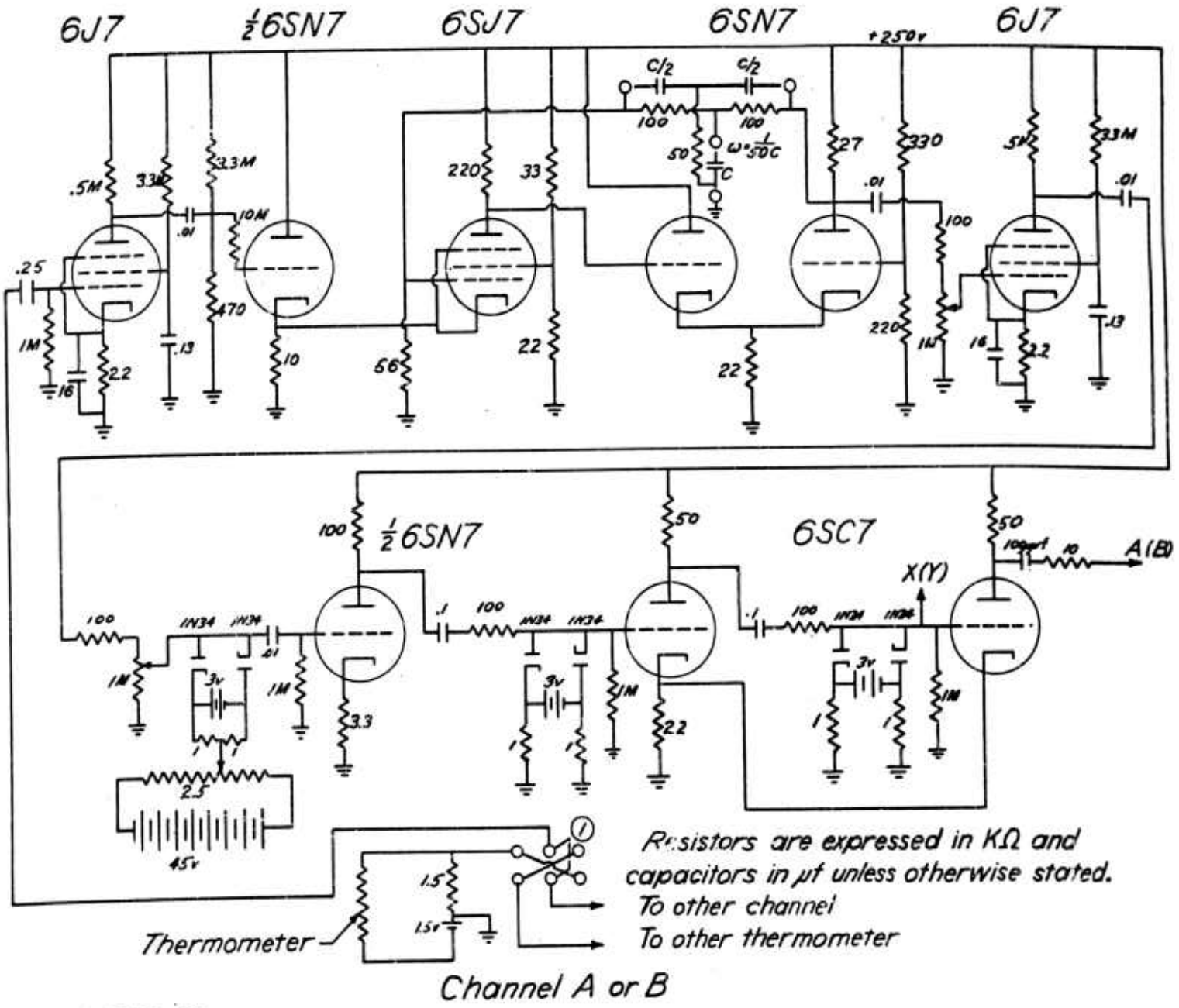
6J7
½6SN7
6SJ7
6SN7
6J7
+250v
C/2
C/2
100
100
50
ω=1/50C
C
.5M
3.3M
.01
10M
.25
1M
.1
470
10
220
33
56
22
22
27
330
.01
100
220
1M
.5M
33M
.01
.1
16
2.2
100
½6SN7
50
6SC7
50
A(B)
X(Y)
100
1N34
1N34
.01
1M
3v
1M
3.3
.1
100
1N34
1N34
3v
1M
22
.1
100
1N34
1N34
3v
1M
2.5
45v
1.5
1.5v
Thermometer
Resistors are expressed in KΩ and
capacitors in μf unless otherwise stated.
To other channel
To other thermometer
Channel A or B

FIGURE 27

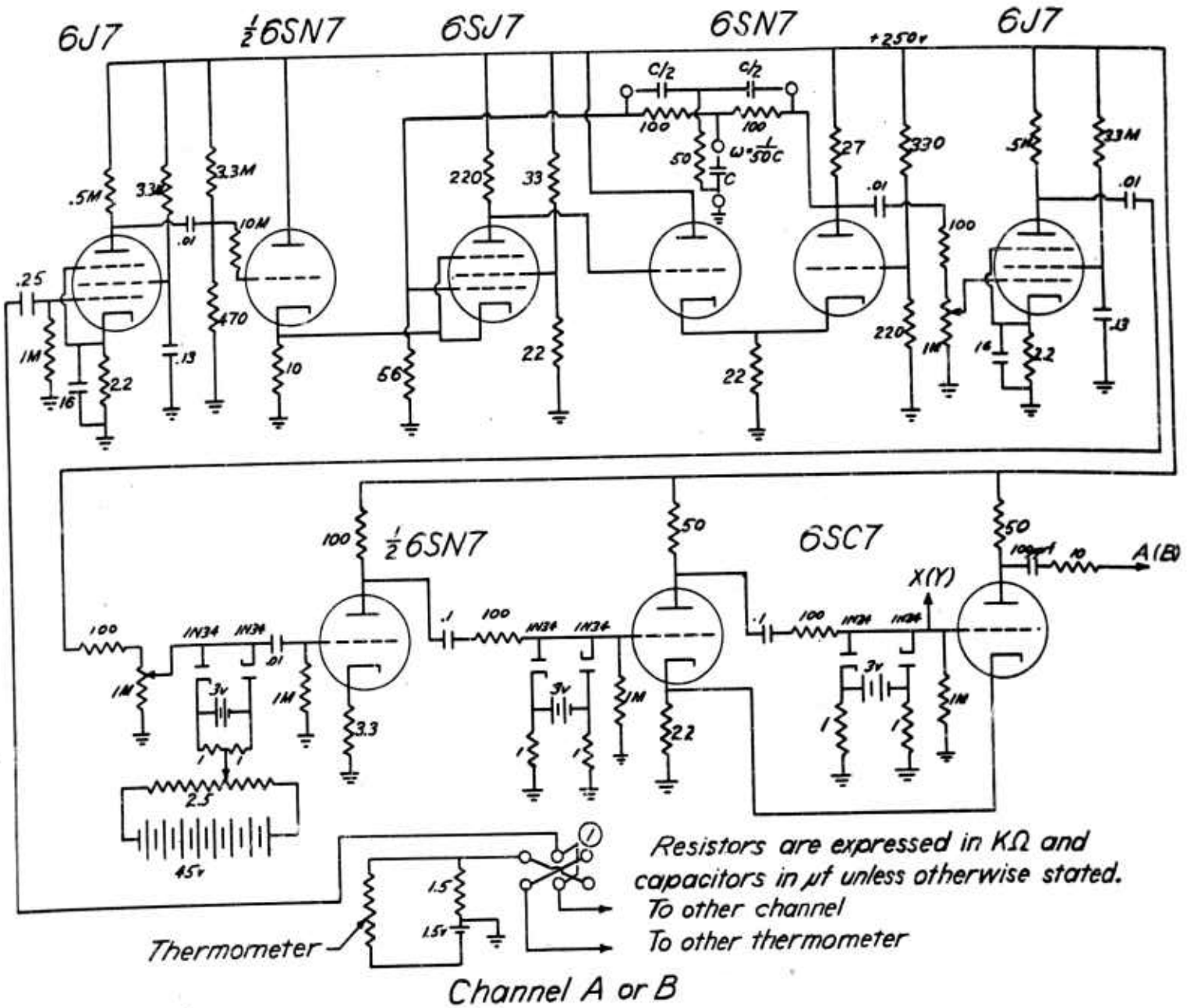
6J7
½6SN7
6SJ7
6SN7
6J7
+250v
C/2
C/2
100
100
50
ω=1/50C
C
27
330
.5M
33M
.01
.5M
33M
10M
.01
220
33
100
.25
470
.13
1M
22
16
10
56
22
22
220
1M
16
22
.13
100
½6SN7
50
6SC7
50
A(B)
X(Y)
100
1N34
1N34
.01
.1
100
1N34
1N34
.1
100
1N34
1N34
1M
3v
1M
3.3
1M
22
1M
2.5
45v
1.5
1.5v
Thermometer
Resistors are expressed in KΩ and
capacitors in μf unless otherwise stated.
To other channel
To other thermometer
Channel A or B

FIGURE 27

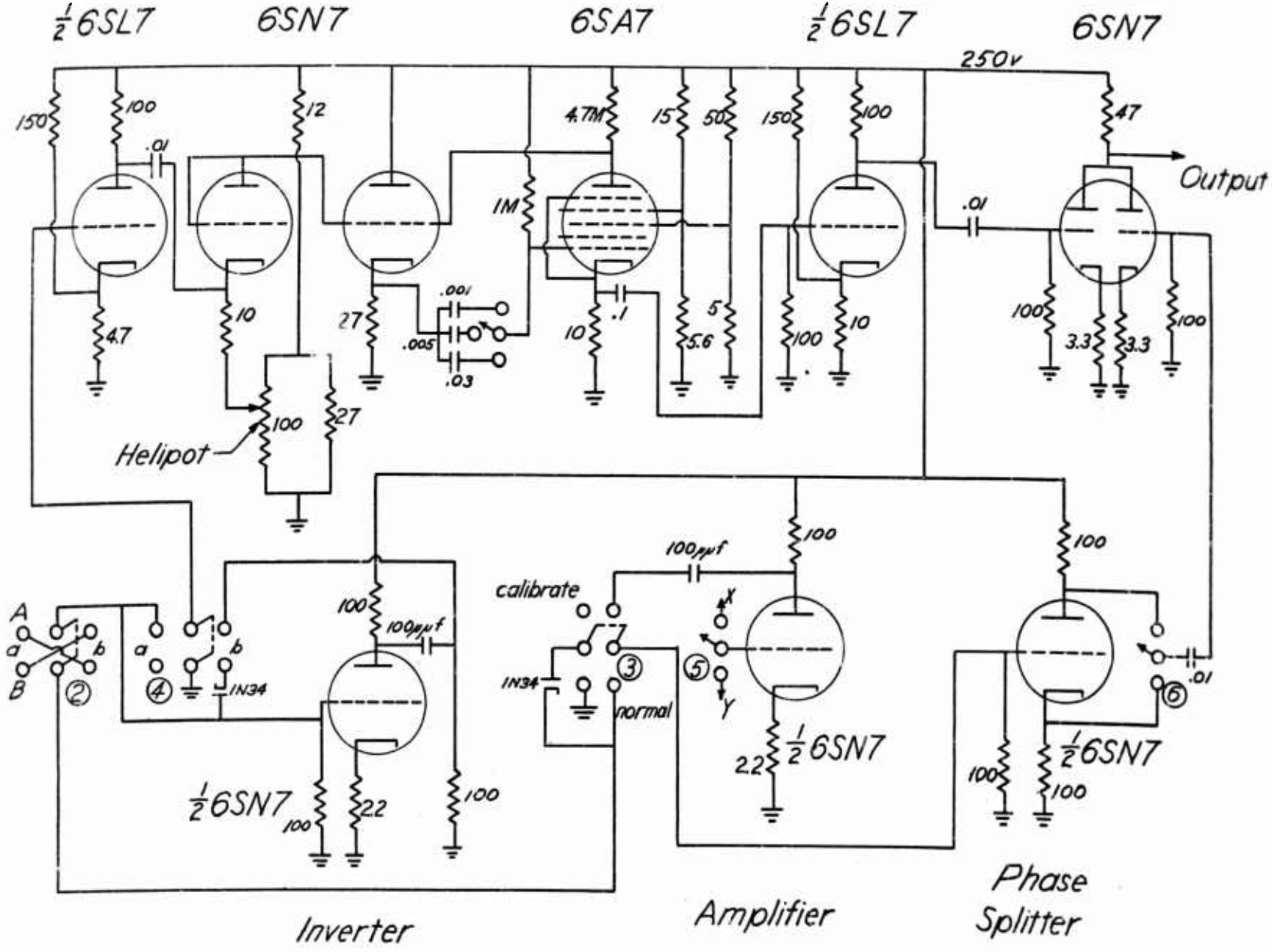
½6SL7
6SN7
6SA7
½6SL7
6SN7
250v
150
100
.01
12
4.7M
15
50
150
100
47
Output
.01
1M
.001
.005
.03
27
10
4.7
10
.1
5
5.6
100
10
100
3.3
3.3
100
Helipot
100
27
A
B
a
b
a
b
IN34
100
100μμf
100μμf
calibrate
IN34
normal
X
Y
100
½6SN7
100
22
100
2.2
½6SN7
100
½6SN7
100
100
.01
Inverter
Amplifier
Phase
Splitter

FIGURE 28

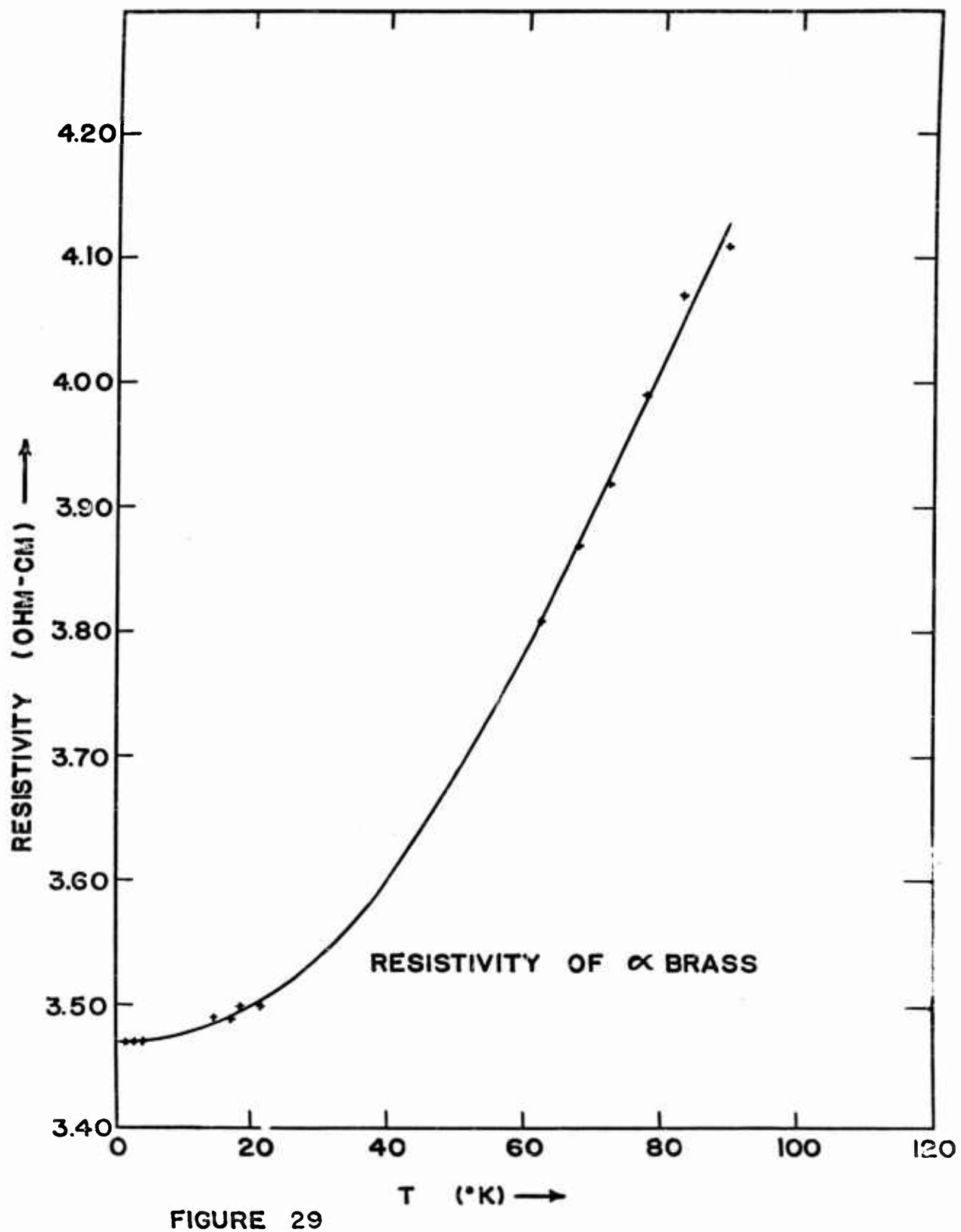
4.20
4.10
4.00
3.90
3.80
3.70
3.60
3.50
3.40
RESISTIVITY (OHM-CM) ⟶
RESISTIVITY OF ∝ BRASS
0
20
40
60
80
100
120
T (°K) ⟶

FIGURE 29

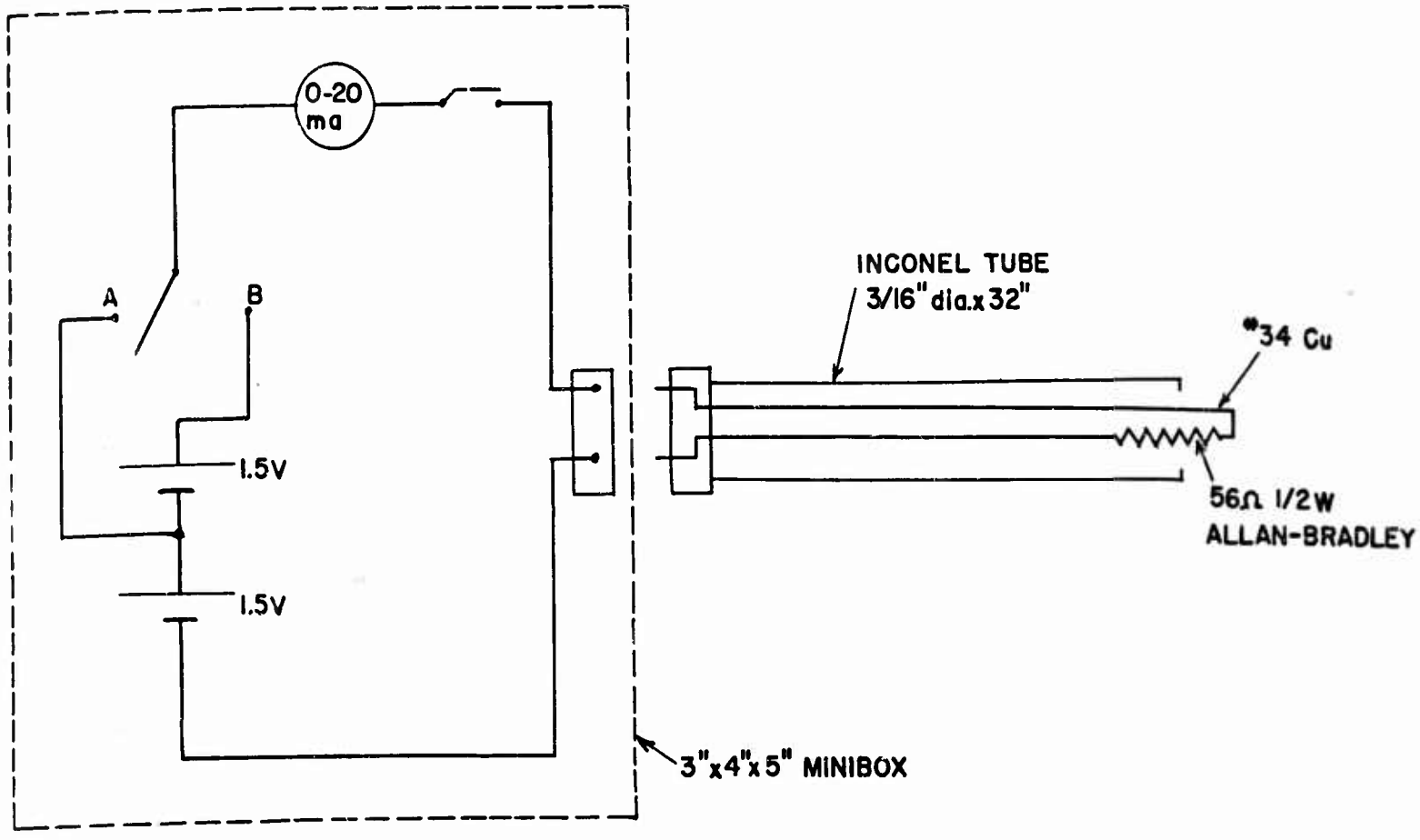

LIQUID LEVEL INDICATOR FOR : He, H_2, N_2

FIGURE 30

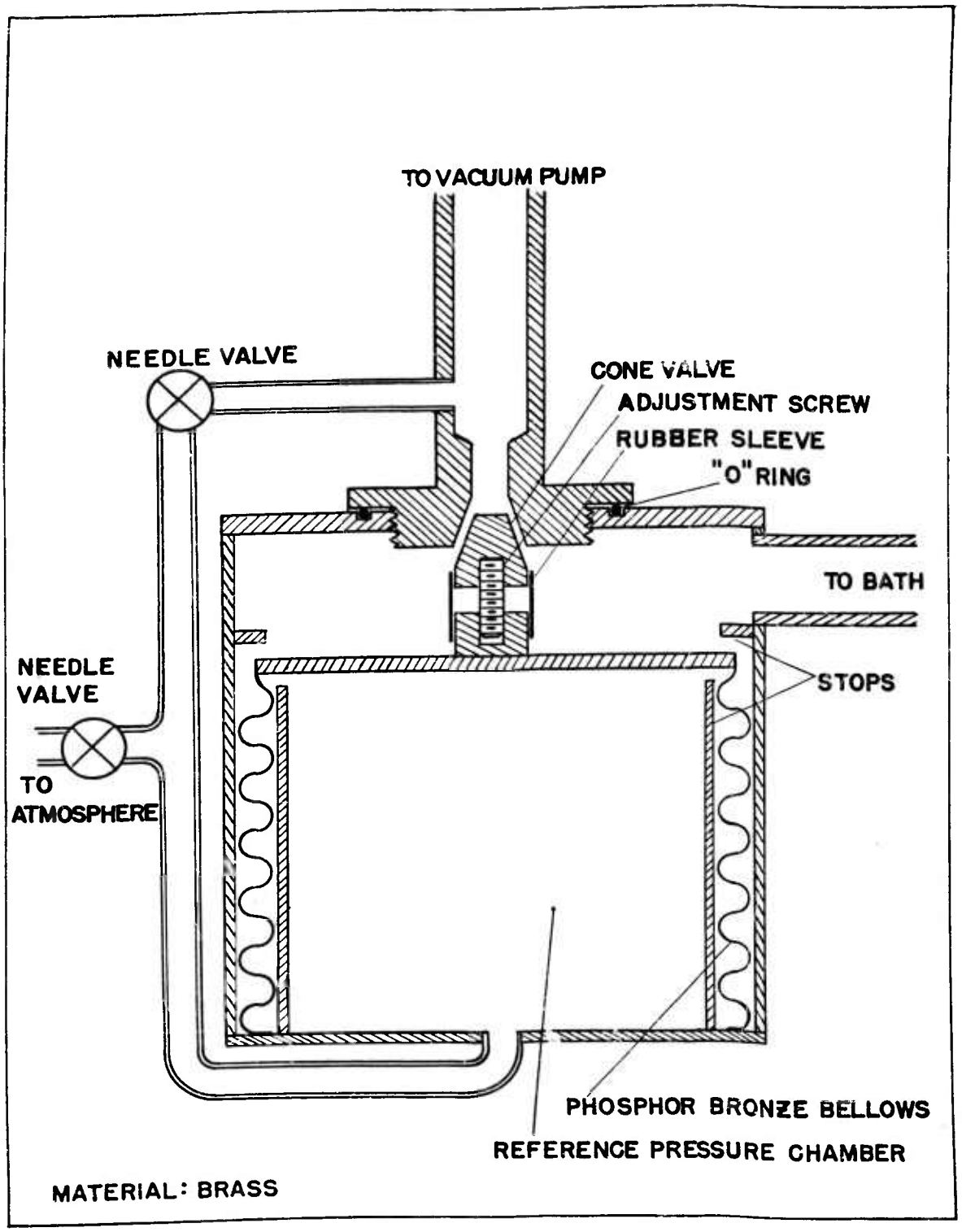

FIGURE 31 BELLOWS PRESSURE MANOSTAT - CROSS SECTION